Particle Detection: Trackers

Lecture 1

Gregor Herten

University of Freiburg, Germany

09. June 2009

CERN-FNAL HCP School 2009

Outline

Lecture 1

1. Interaction of charged particle with matter
2. Momentum measurement
3. Drift and Diffusion in Gases
4. History of Tracking Detectors (not shown)
5. Proportional Chambers

Lecture 2

6. Drift Chambers
7. Micro Pattern Gas Chambers
8. Limitations of Gaseous Detectors

Lecture 3

9. Vertex Reconstruction
10. Semiconductor Detectors
11. Silicon Strip and Pixel Detectors
12. Radiation Damage of Silicon Detectors
13. New Semiconductor Detector Concepts
14. Tracking Systems: ATLAS, CMS

1. Interaction of Particle with Matter

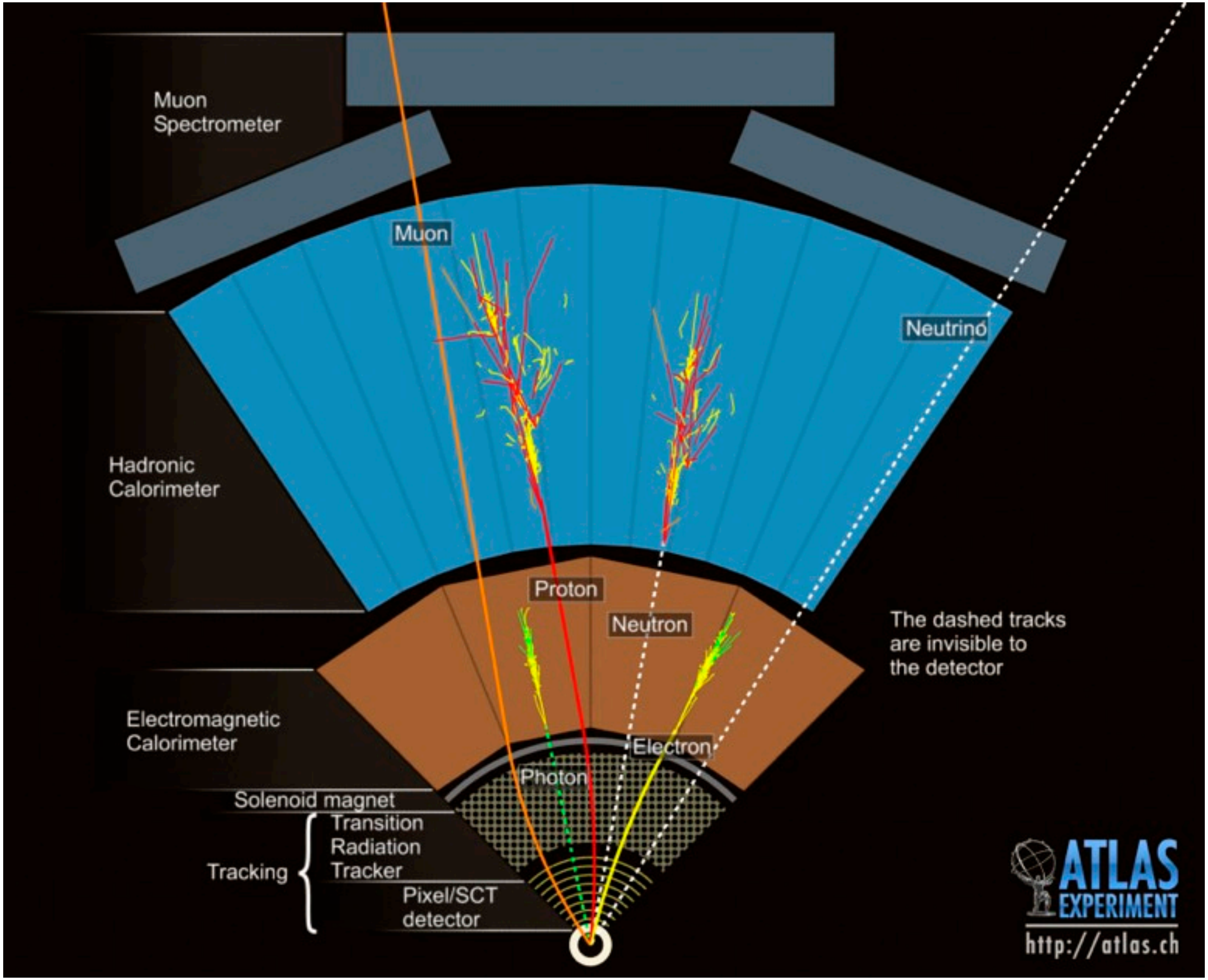

Challenge in Tracking

e+ e- collision in the ALEPH Experiment/LEP.

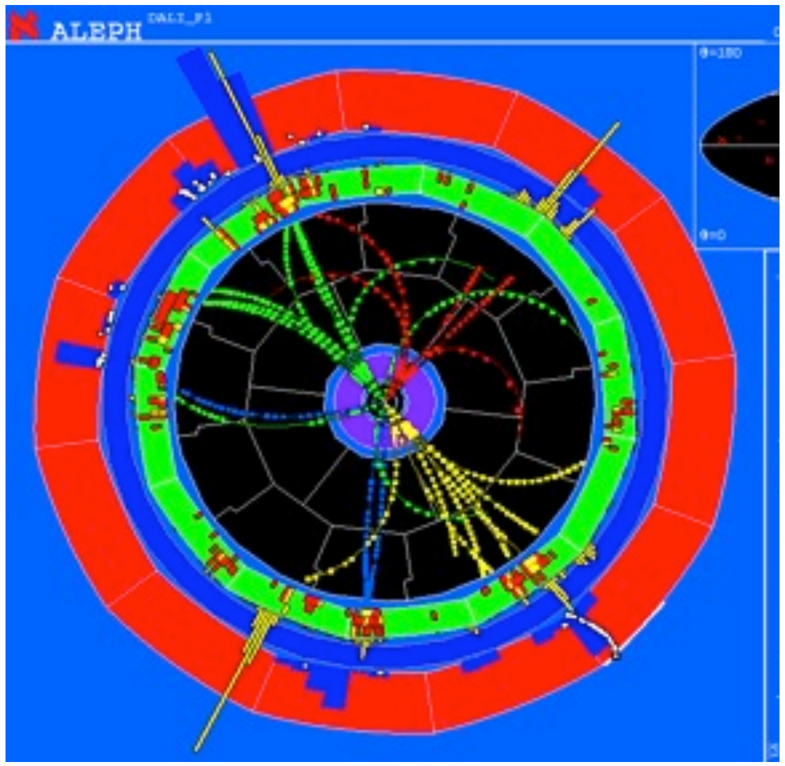

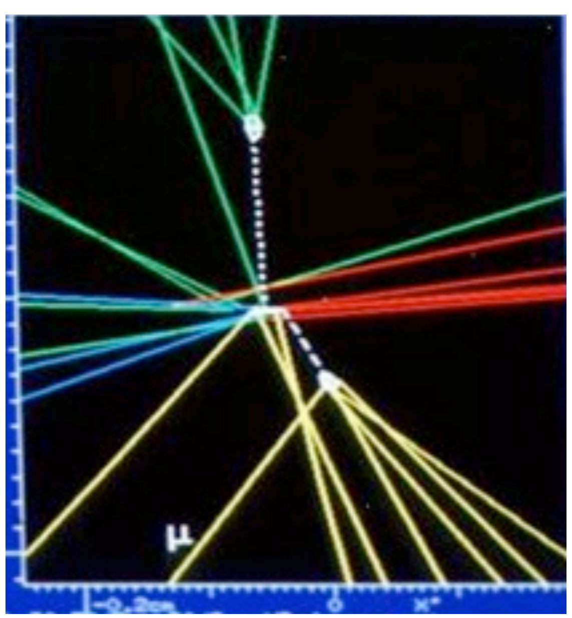

Au+ Au+ collision in the STAR Experiment/RHIC

Up to 2000 tracks

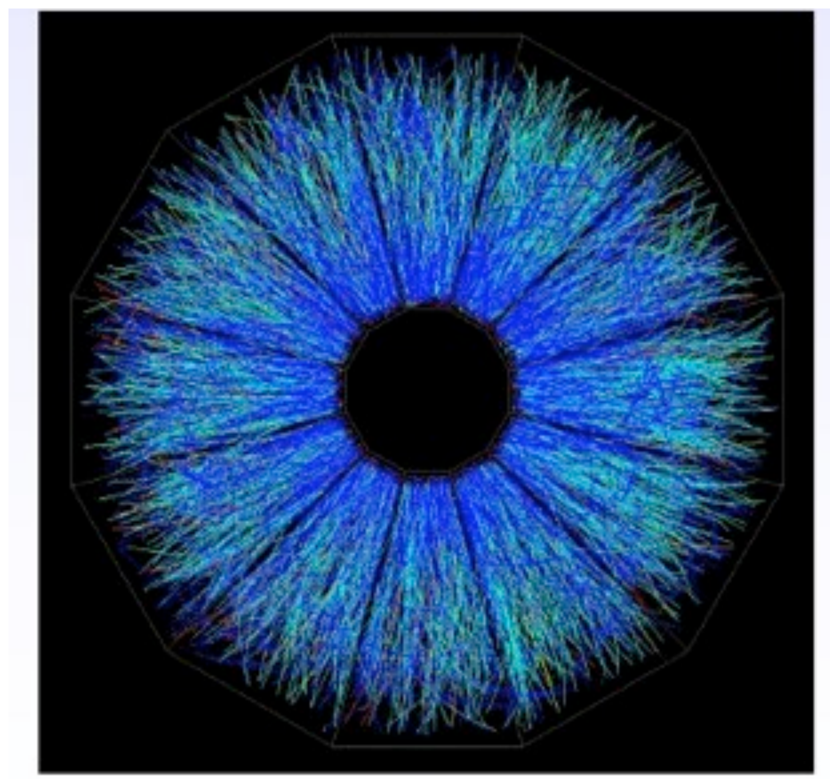

Pb+ Pb+ Kollision in the ALICE Experiment/LHC

Simulation for

Angle Θ=60 to 62º

Up to 40 000 tracks/collision

1. Energy Loss of Charged Particle by Atomic Collisions

A charged particle passing through matter suffers
1. energy loss
2. deflection from incident direction

Main type of reactions:
1. Inelastic collisions with atomic electrons of the material.
2. Elastic scattering from nuclei.

Less important reactions are:
3. Emission of Cherenkov radiation
4. Nuclear reactions
5. Bremsstrahlung

Classification of charged particles with respect to interaction with matter:
1. Low mass: electrons and positrons
2. High mass: muons, pions, protons, light nuclei.

Energy loss:
- mainly due to inelastic collisions with atomic electrons.
- cross section $\sigma \cong 10^{-17} - 10^{-16}$ cm^2 !
- small energy loss in each collision, but many collisions in dense material. Thus one can work with average energy loss.
- Example: a proton with E_{kin}=10 MeV looses all its energy after 0.25 mm of copper.

Two groups of inelastic atomic collisions:
- soft collisions: only excitation of atom.
- hard collisions: ionization of atom. In some of the hard collisions the atomic electron get such a large energy that it causes secondary ionisation (δ-electrons).

Elastic collisions from nuclei cause very small energy loss. They are the main cause for deflection.

1. Bethe-Bloch Formula

Bethe-Bloch formula gives the mean rate of energy loss (stopping power) of a heavy charged particle.

$$-\frac{dE}{dx} = Kz^2 \frac{Z}{A} \frac{1}{\beta^2} \left[\frac{1}{2} \ln \frac{2m_e c^2 \beta^2 \gamma^2 T_{max}}{I^2} - \beta^2 - \frac{\delta(\beta\gamma)}{2} \right]$$

PDG 2008

with

A : atomic mass of absorber

$\frac{K}{A} = 4\pi N_A r_e^2 m_e c^2 / A = 0.307075 \text{ MeV g}^{-1}\text{cm}^2, \text{ for A} = 1\text{g mol}^{-1}$

z: atomic number of incident particle

Z: atomic number of absorber

T_{max} : Maximum energy transfer in a single collision $\quad T_{max} = \frac{2m_e c^2 \beta^2 \gamma^2}{1+2\gamma m_e/M + (m_e/M)^2}$

δ(βγ) : density effect correction to ionization loss.

x = ρ s , surface density or mass thickness, with unit g/cm², where s is the length.

dE/dx has the units MeV cm²/g

1. History of Energy Loss Calculations: dE/dx

(not shown)

1915: Niels Bohr, classical formula, Nobel prize 1922.
1930: Non-relativistic formula found by Hans Bethe
1932: Relativistic formula by Hans Bethe

Bethe's calculation is leading order in pertubation theory, thus only z^2 terms are included.

Additional corrections:

- z^3 corrections calculated by Barkas-Andersen
- z^4 correction calculated by Felix Bloch (Nobel prize 1952, for nuclear magnetic resonance). Although the formula is called Bethe-Bloch formula the z^4 term is usually not included.
- Shell corrections: atomic electrons are not stationary
- Density corrections: by Enrico Fermi (Nobel prize 1938, for discovery of nuclear reaction induced by slow neutrons).

Hans Bethe
1906-2005

Born in Strasbourg, emigrated to US in 1933. Professor at Cornell U. Nobel prize 1967 for theory of nuclear processes in stars.

1. Examples of Mean Energy Loss

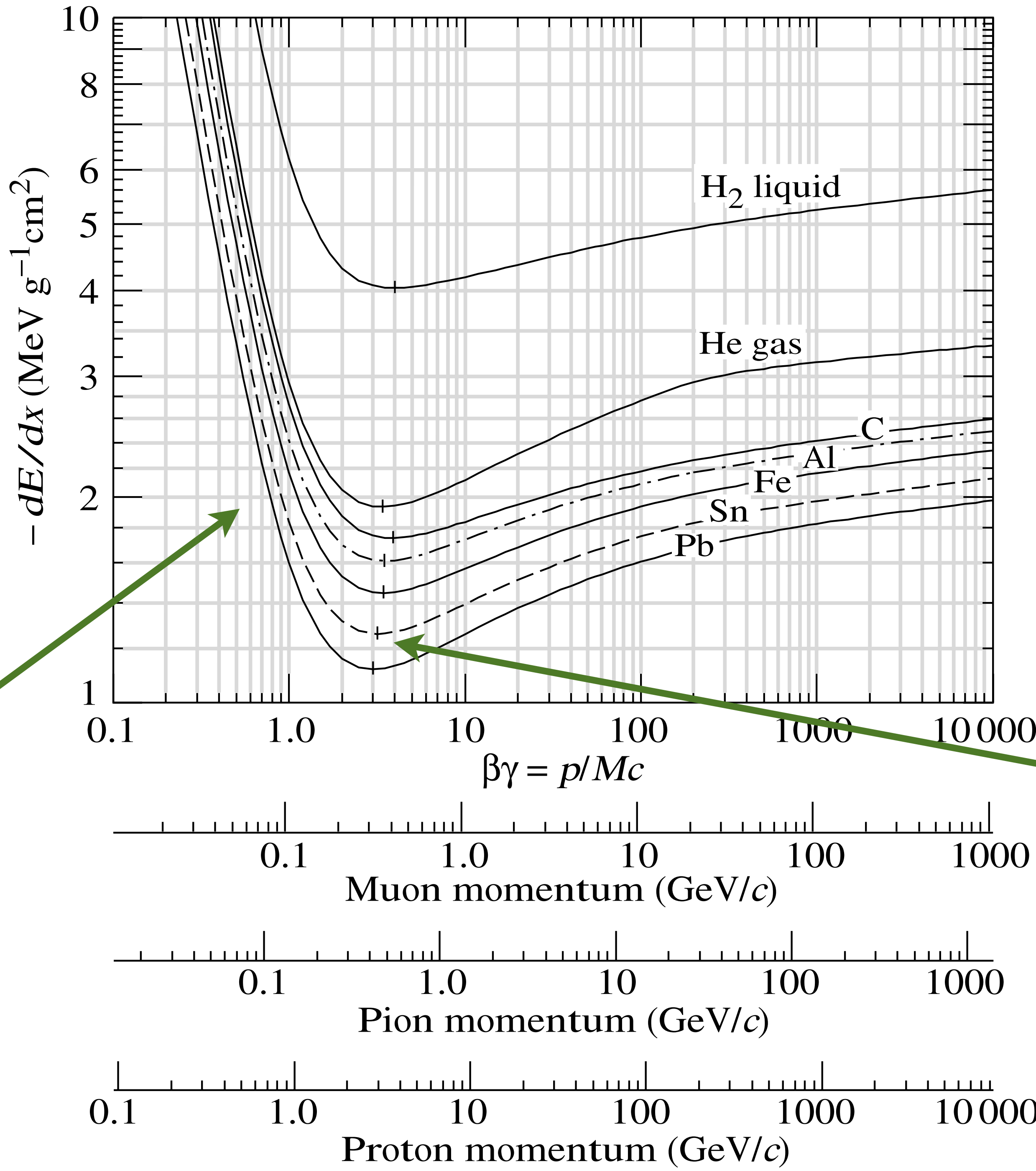

Figure 27.3: Mean energy loss rate in liquid (bubble chamber) hydrogen, gaseous helium, carbon, aluminum, iron, tin, and lead. Radiative effects, relevant for muons and pions, are not included. These become significant for muons in iron for $\beta\gamma \gtrsim 1000$, and at lower momenta for muons in higher-Z absorbers. See Fig. 27.21.

$1/\beta^2$

Bethe-Bloch formula:

$$-\frac{dE}{dx} = K z^2 \frac{Z}{A} \frac{1}{\beta^2} \left[\frac{1}{2} \ln f(\beta) - \beta^2 - \frac{\delta(\beta\gamma)}{2}\right]$$

Except in hydrogen particles of the same velocity have similar energy loss in different materials.

The minimum in ionization occurs at

$\beta\gamma$=3.5 to 3.0,

as Z goes from 7 to 100

PDG 2008

1. Particle Identification from dE/dx and p Measurements

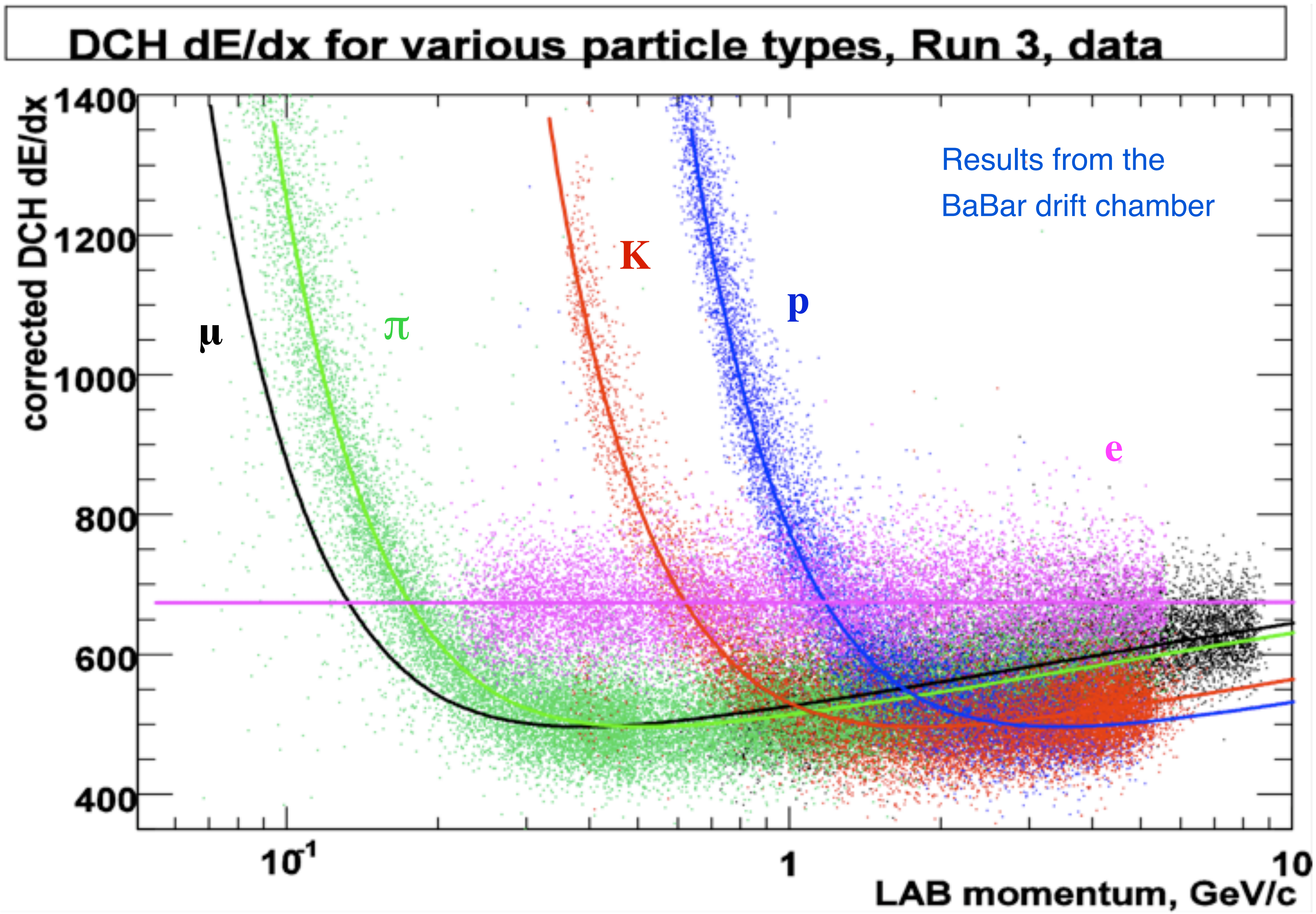

A simultaneous measurement of dE/dx and momentum can provide particle identification.

1. Fluctuations in Energy Loss

Real detector (limited granularity) can not measure <*dE/dx*> !

It measures the energy ΔE deposited in a layer of finite thickness δx.

For thin layers or low density materials:

→ Few collisions, some with high energy transfer.

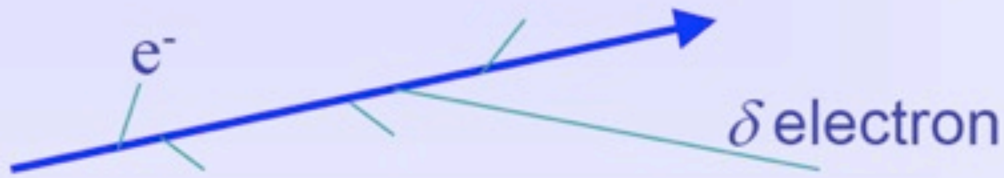

→ Energy loss distributions show large fluctuations towards high losses: "Landau tails"

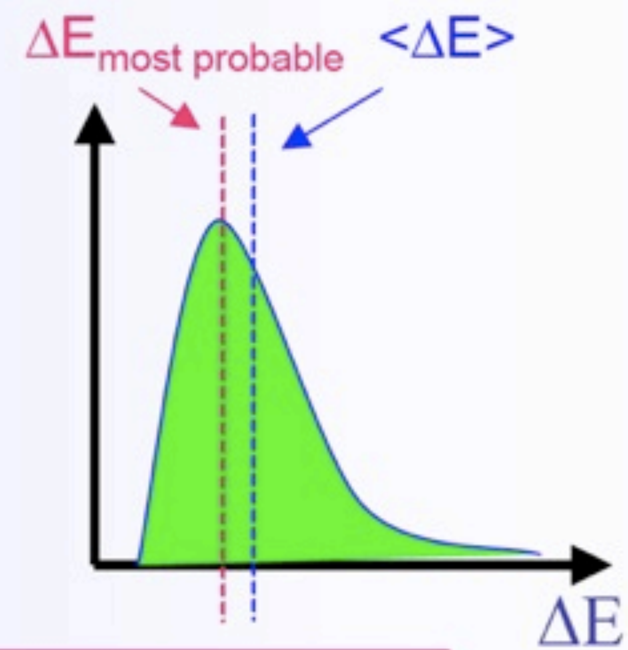

Example: Si sensor: 300 μm thick. $\Delta E_{m.p} \sim 82$ keV $<\Delta E> \sim 115$ keV

For thick layers and high density materials:

→ Many collisions.

→ Central Limit Theorem → Gaussian shaped distributions.

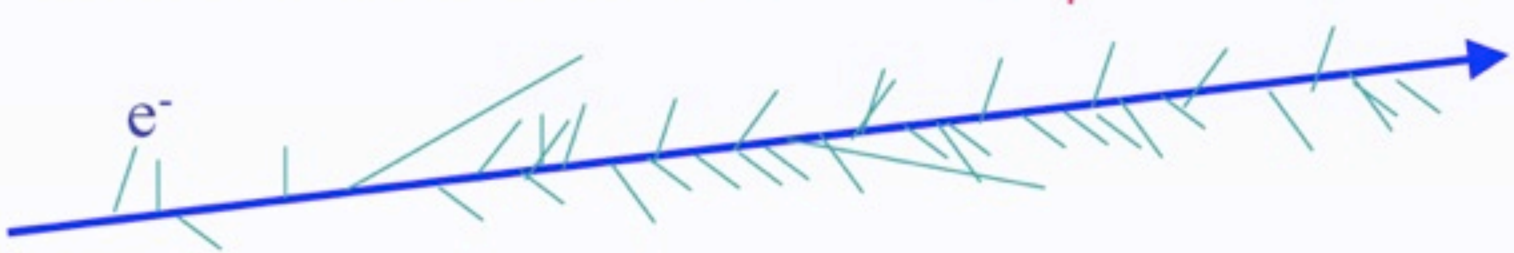

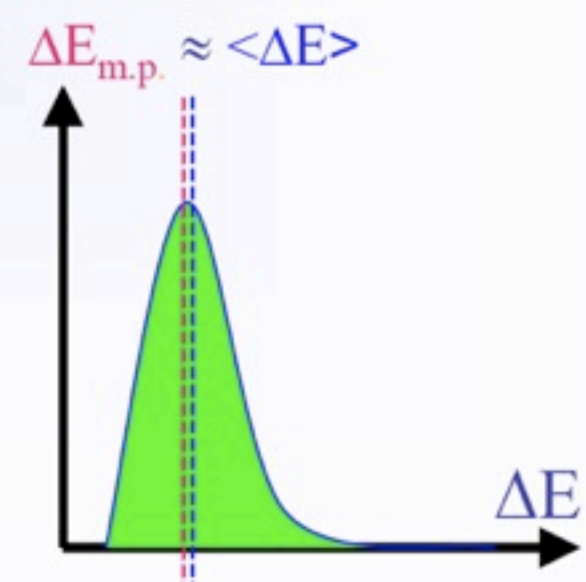

from L. Ropelewski

1. Bremsstrahlung

High energy electrons loose their energy predominantly through radiation (bremsstrahlung).

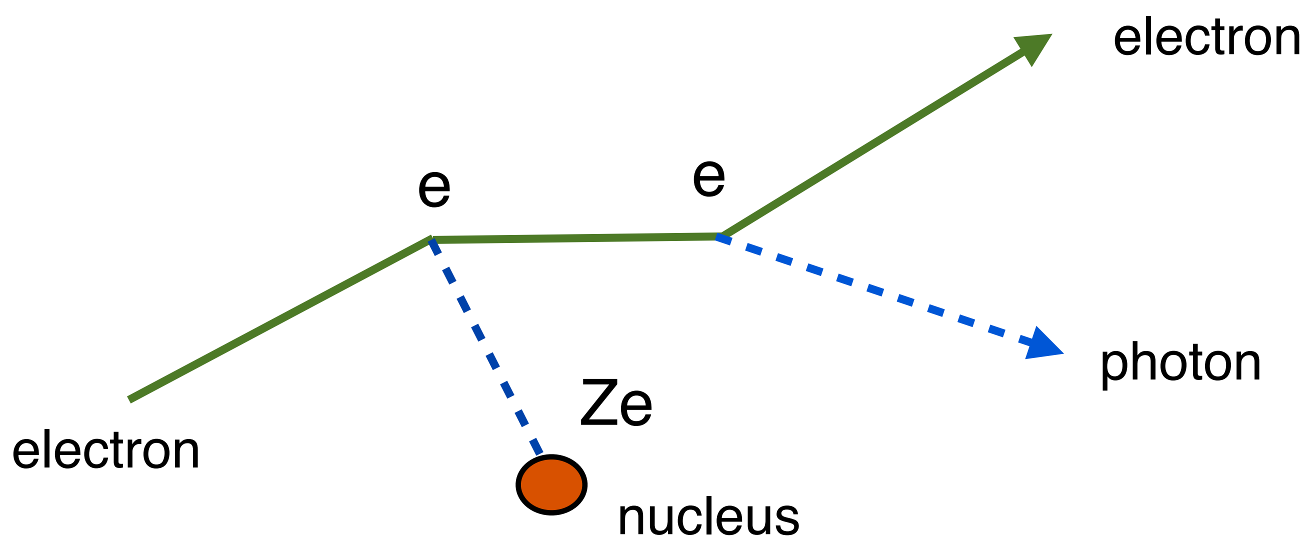

Cross section:

$$\sigma \sim (Z\, e^3)^2 \sim Z^2 \;\; \alpha^3$$

The electron is decelerated (accelerated) in the field of the nucleus. Accelerated charges radiate photons. Thus the bremsstrahlung is strong for light charged particles (electrons), because its acceleration is large for a given force. For heavier particles like muons bremsstrahlung effects are only important at energies of a few hundred GeV.

The presence of a nucleus is required to restore energy-momentum conservation. Thus the cross section is proportional to Z^2 and α^3 (α = fine structure constant).

The characteristic length which a electron travels in material until a bremsstrahlung happens is the radiation length X_0.

1. Radiation Length X_0

The radiation length is the characteristic length scale to describe electromagnetic showers in material. It is usually measured in g/cm^2.

The radiation length is:
- the mean distance over which a high energy electron looses all but 1/e of its energy.
- 7/9 of the mean free path for pair production by a high energy photon.

The radiation length is give by:

$$\boxed{\frac{1}{X_0} = 4\alpha r_e^2 \frac{N_A}{A} \left\{ Z^2 \left[L_{\text{rad}} - f(Z) \right] + Z\, L'_{\text{rad}} \right\}}$$

For $A = 1$ g mol^{-1}, $4\alpha r_e^2 N_A / A = (716.408 \text{ g cm}^{-2})^{-1}$.

$$f(Z) = a^2 \left[(1 + a^2)^{-1} + 0.20206 - 0.0369\, a^2 + 0.0083\, a^4 - 0.002\, a^6 \right]$$

where $a = \alpha Z$

Element	Z	L_{rad}	L'_{rad}
H	1	5.31	6.144
He	2	4.79	5.621
Li	3	4.74	5.805
Be	4	4.71	5.924
Others	> 4	$\ln(184.15\, Z^{-1/3})$	$\ln(1194\, Z^{-2/3})$

1. High Energy Muon Bremsstrahlung

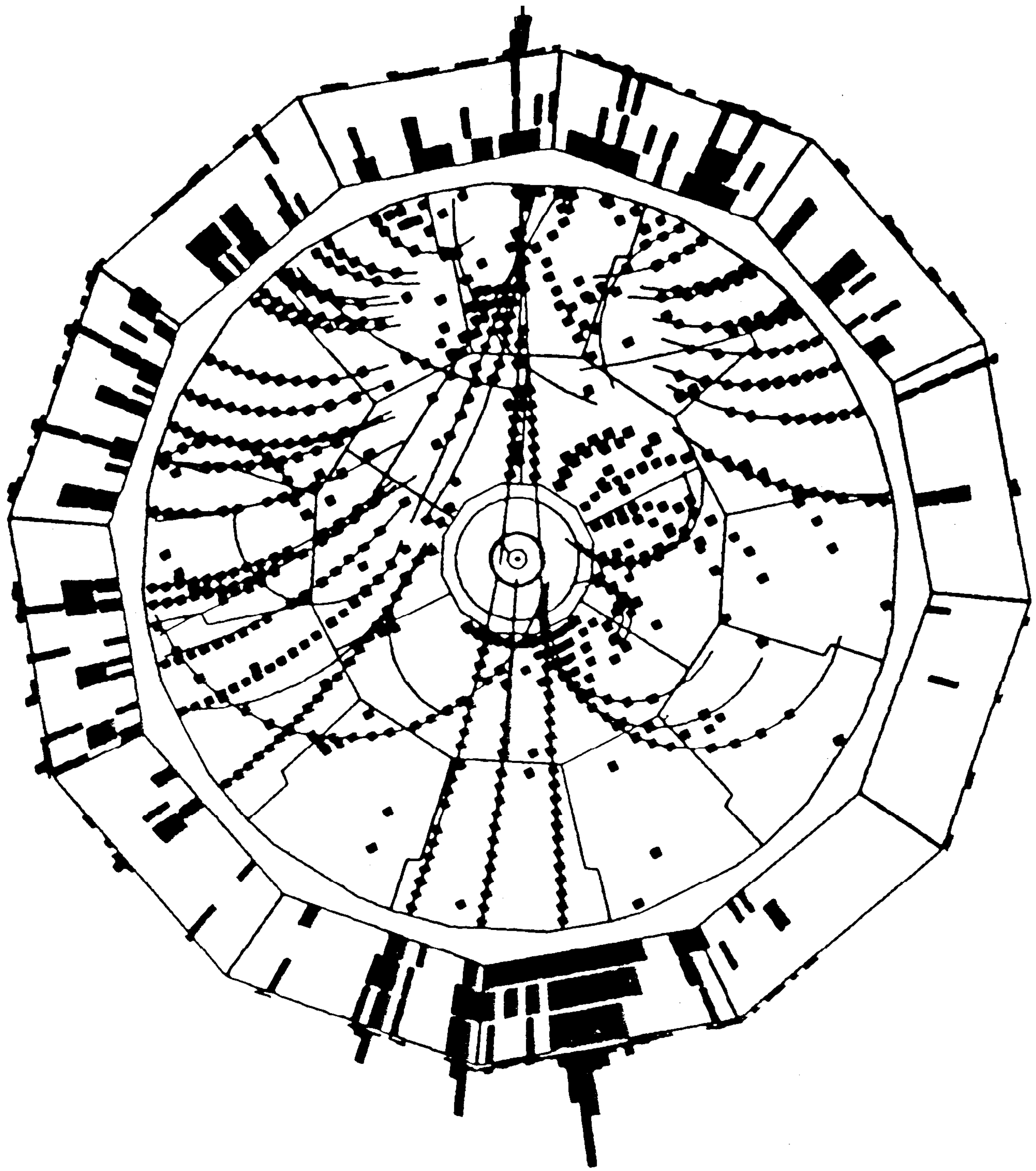

Bremsstrahlung off muons starts to be important for momenta of a few hundred GeV.

Cosmic muon bremsstrahlung event in the ALEPH detector at LEP.

1. Multiple Coulomb Scattering

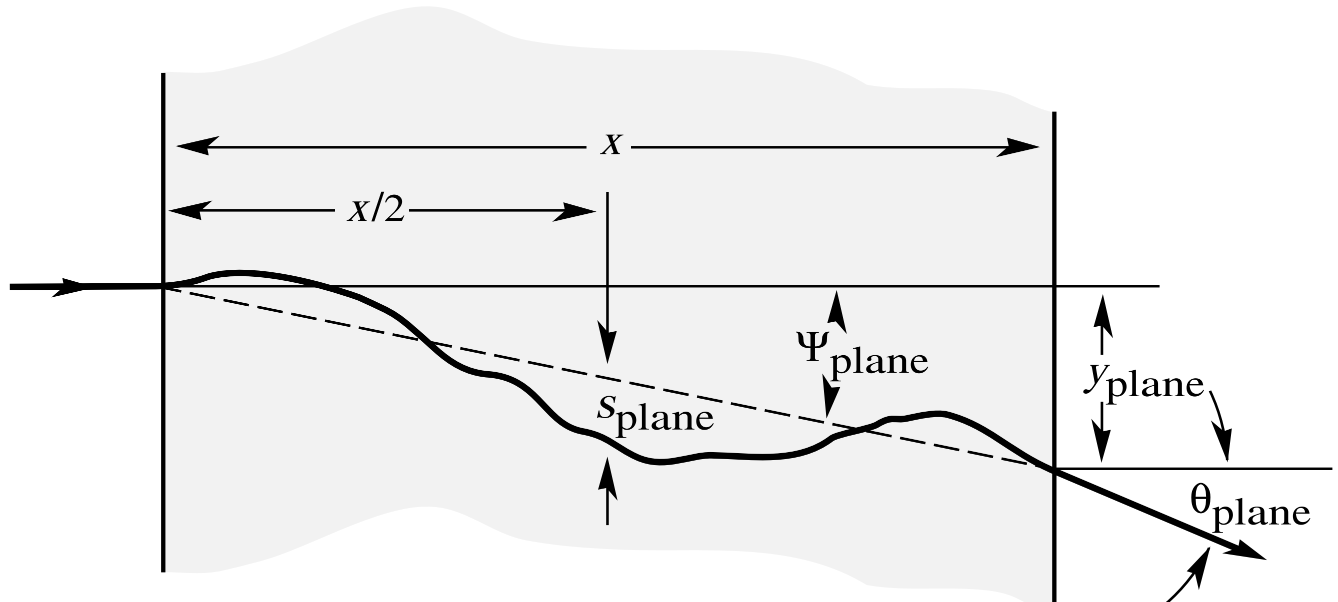

Figure 27.9: Quantities used to describe multiple Coulomb scattering. The particle is incident in the plane of the figure.

$$\psi^{\text{rms}}_{\text{plane}} = \frac{1}{\sqrt{3}}\,\theta^{\text{rms}}_{\text{plane}} = \frac{1}{\sqrt{3}}\,\theta_0 \ ,$$

$$y^{\text{rms}}_{\text{plane}} = \frac{1}{\sqrt{3}}\,x\,\theta^{\text{rms}}_{\text{plane}} = \frac{1}{\sqrt{3}}\,x\,\theta_0 \ ,$$

$$s^{\text{rms}}_{\text{plane}} = \frac{1}{4\sqrt{3}}\,x\,\theta^{\text{rms}}_{\text{plane}} = \frac{1}{4\sqrt{3}}\,x\,\theta_0 \ .$$

A particle which traverses a medium is deflected by small angle Coulomb scattering from nuclei. For hadronic particles also the strong interaction contributes.

The angular deflection after traversing a distance x is described by the Molière theory.
The angle has roughly a Gauss distribution, but with larger tails due to Coulomb scattering.

Defining: $\theta_0 = \theta^{\text{rms}}_{\text{plane}} = \frac{1}{\sqrt{2}}\,\theta^{\text{rms}}_{\text{space}}$

Gaussian approximation:

$$\boxed{\theta_0 = \frac{13.6\ \text{MeV}}{\beta c p}\, z\, \sqrt{x/X_0}\Big[1 + 0.038\ln(x/X_0)\Big]}$$

x/X_0 is the thickness of the material in radiation length.

2. Momentum measurement in B-Fields

The momentum is measured from the sagitta s, which gives the curvature ρ of the track in the magnetic field.

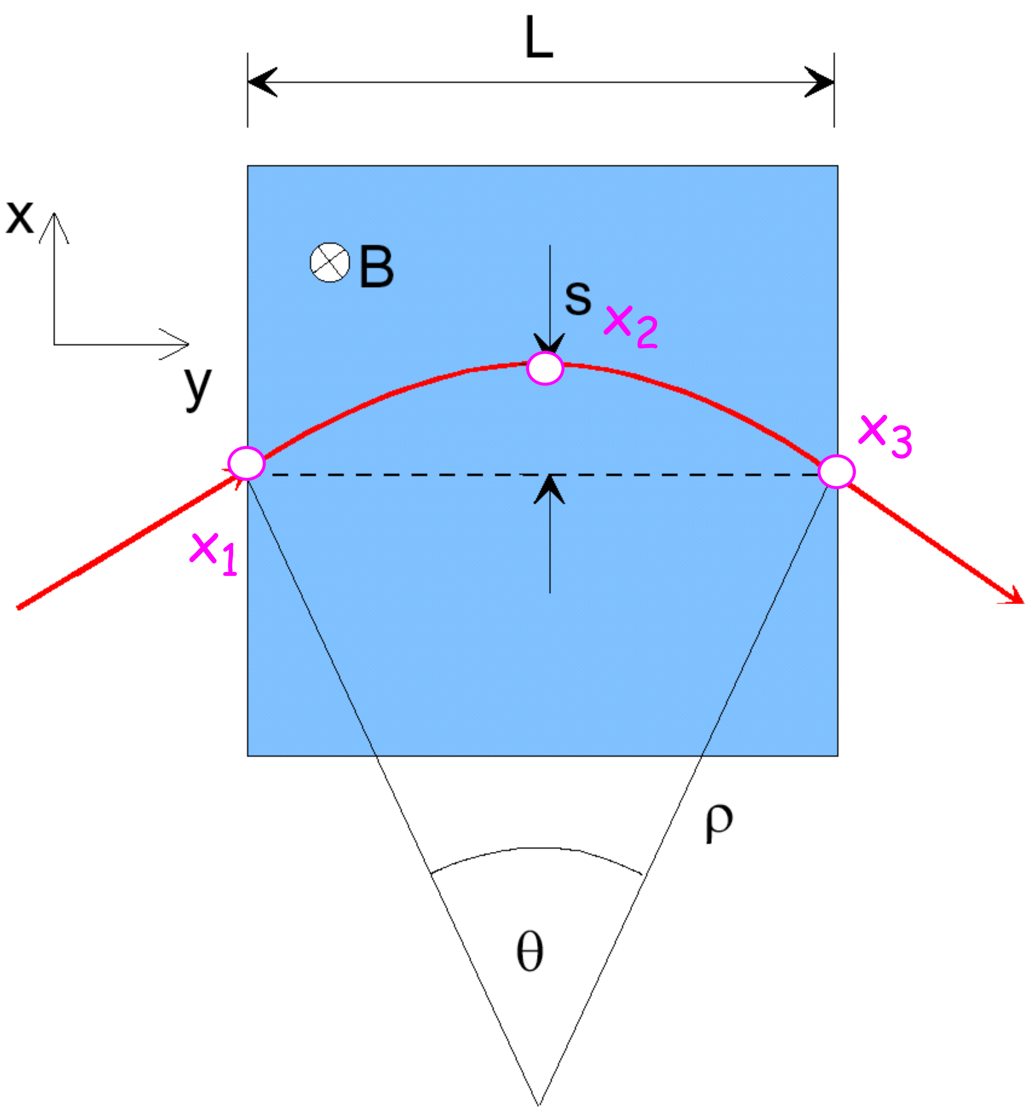

Transverse momentum:

$$p_T = qB\rho$$

$$p_T[GeV] = 0.3\ B[T]\ \rho[m]$$

$$\frac{L/2}{\rho} = \sin\frac{\theta}{2} \approx \frac{\theta}{2}\ \text{(for small } \theta) \Rightarrow \theta \approx \frac{L}{\rho} = \frac{0.3BL}{p_T}$$

$$s = \rho(1-\cos\frac{\theta}{2}) \approx \rho\left(1-(1-\frac{1}{2}\frac{\theta^2}{4})\right) = \rho\frac{\theta^2}{8} \approx \frac{0.3BL^2}{8p_T}$$

Example: 3 measurements

$$s = x_2 - (x_1+x_3)/2 \rightarrow ds = dx_2 - dx_1/2 - dx_3/2$$

assume uncorrelated errors: $\sigma(x) \approx dx_i$

$$\sigma_s^2 = \sigma^2(x) + 2\frac{\sigma^2(x)}{4} = \frac{3}{2}\sigma^2(x)$$

2. Relative Momentum Error

For 3 points the relative momentum resolution is given by: $\frac{\sigma(p_T)}{p_T} = \frac{\sigma_s}{s} = \sqrt{\frac{3}{2}}\sigma(x) \cdot \frac{8 p_T}{0.3BL^2}$

- degrades linearly with transverse momentum
- improves linearly with increasing B field
- improves quadratically with radial extension of detector

In the case of N equidistant measurements according to Gluckstern [NIM 24 (1963) 381]:

$$\boxed{\frac{\sigma(p_T)}{p_T} = \frac{\sigma(\kappa)}{\kappa} = \frac{\sigma(x) \cdot p_T}{0.3BL^2}\sqrt{\frac{720}{(N+4)}}}$$

(for $N \geq 10$, curvature $\kappa = 1/\rho$)

Example: For $p_T = 1\mathrm{GeV}$, $L = 1\mathrm{m}$, $B = 1\mathrm{T}$, $\sigma(x) = 200\mu\mathrm{m}$ and $N = 10$ one obtains:

$$\frac{\sigma(p_T)}{p_T} \approx 0.5\% \quad \text{for a sagitta} \quad s \approx 3.8\mathrm{cm}$$

Important track detector parameter: $\frac{\sigma(p_T)}{p_T^2}$ (%/GeV)

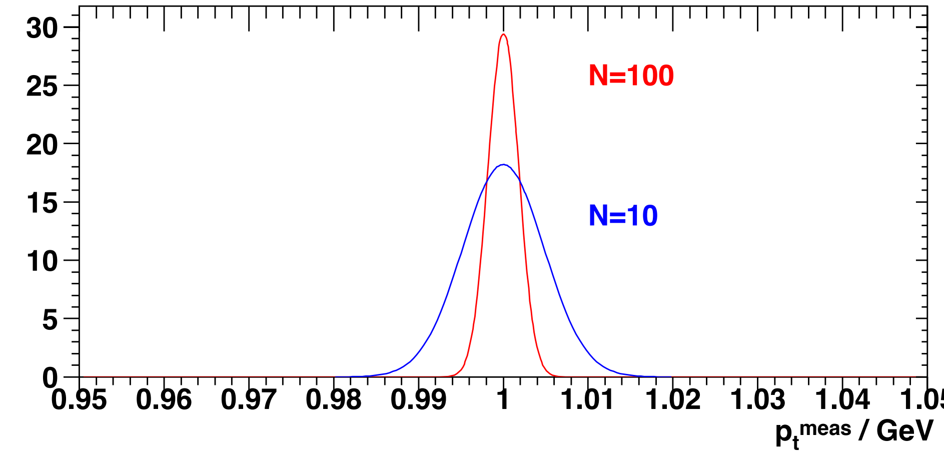

from K. Niebuhr

2. Contributions from Multiple Scattering

The contribution to the momentum error from MS is given by:

$$\left.\frac{\sigma(p_T)}{p_T}\right|_{MS} = \frac{\sigma^{MS}(s)}{s} = \frac{\frac{L'}{4\sqrt{3}}\frac{13.6\times10^{-3}}{p\beta}z\sqrt{\frac{L'}{X_0}}}{0.3BL^2z/(8p_T)} = \frac{52.3\times10^{-3}}{\beta B\sqrt{LX_0\sin\theta}}$$

with

$L' = L/\sin\theta$ total path

$p_T = p\sin\theta$

for $\beta \to 1$ this part is momentum independent !

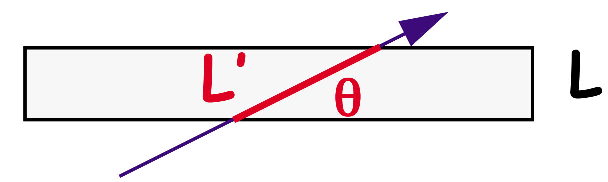

The combined total momentum error is:

$$\boxed{\left(\frac{\sigma_p}{p}\right)^2 = \left(\sqrt{\frac{720}{N+4}}\frac{\sigma_x p\sin\theta}{0.3BL^2}\right)^2 + \left(\frac{52.3\times10^{-3}}{\beta B\sqrt{LX_0\sin\theta}}\right)^2 + (\cot\theta\,\sigma_\theta)^2}$$

Example for momentum dependence of individual contributions

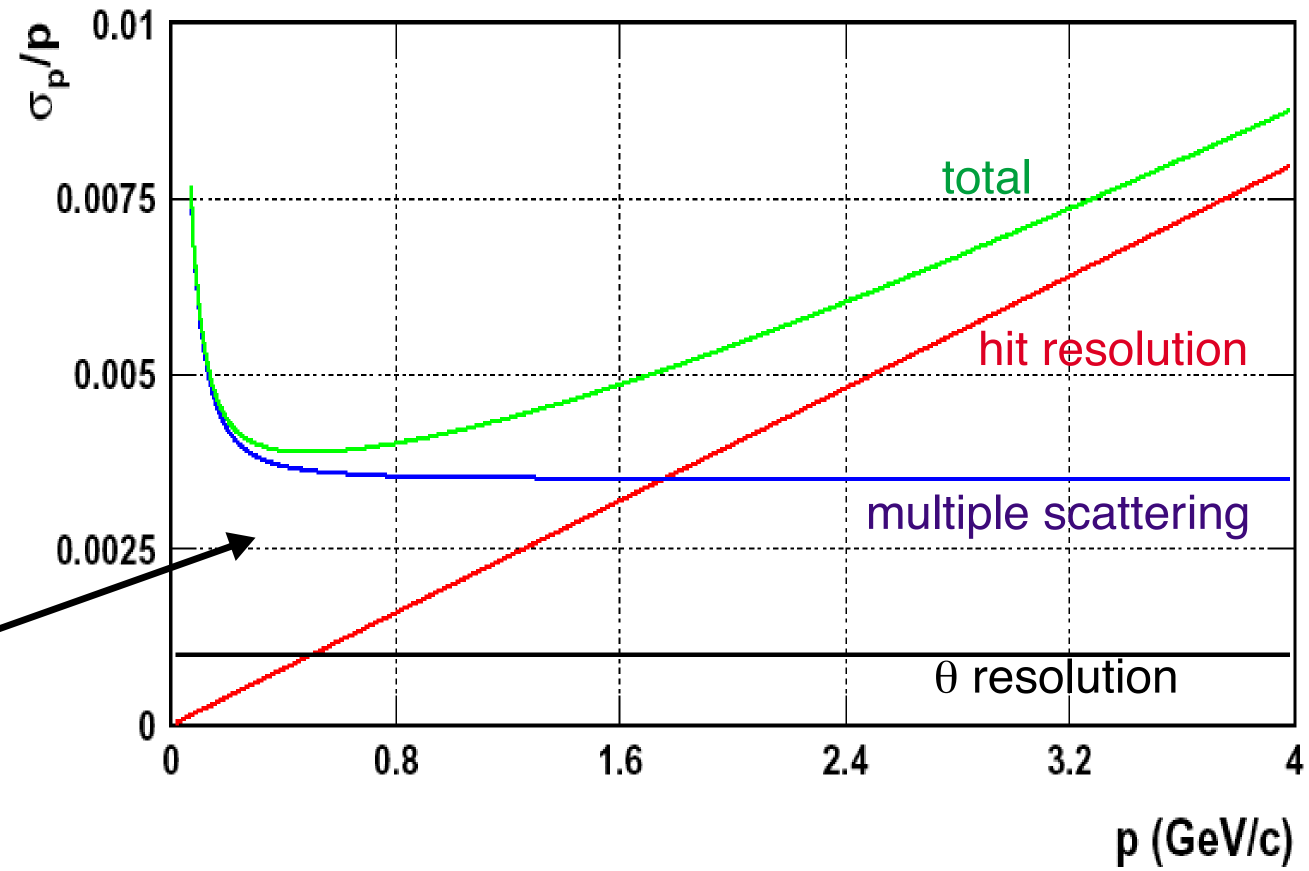

from K. Niebuhr

3 Drift and Diffusion in Gases : Ionization

from L. Ropelewski

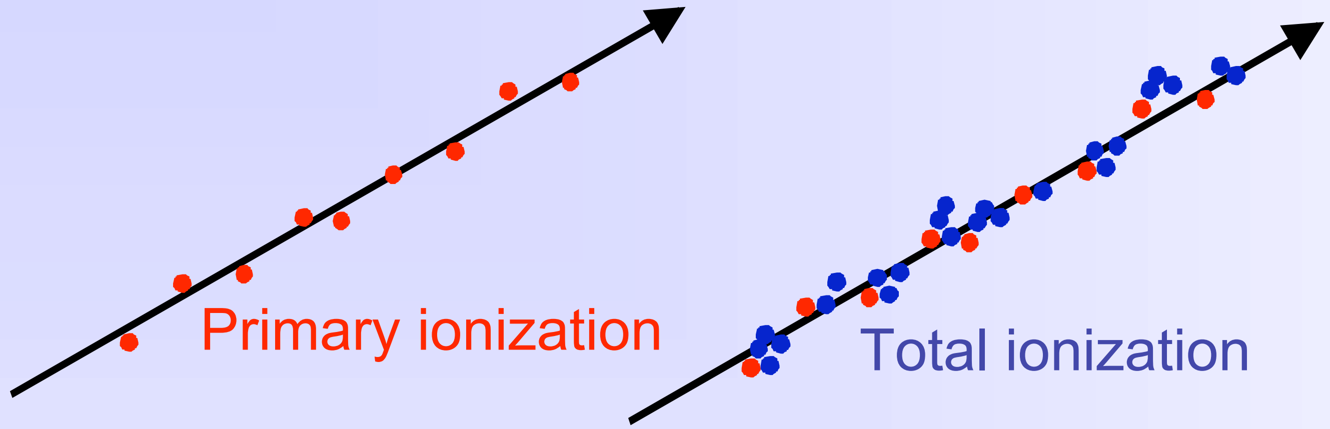

Lohse and Witzeling, Instrumentation In High Energy Physics, World Scientific,1992

Fast charged particles ionize atoms of gas. Often resulting primary electron will have enough kinetic energy to ionize other atoms.

$$n_{total} = \frac{\Delta E}{W_i} = \frac{\frac{dE}{dx}\Delta x}{W_i}$$

$$n_{total} \approx 3 \ldots 4 \cdot n_{primary}$$

n_{total} - number of created electron-ion pairs

Δ_E = total energy loss

W_i = effective <energy loss>/pair

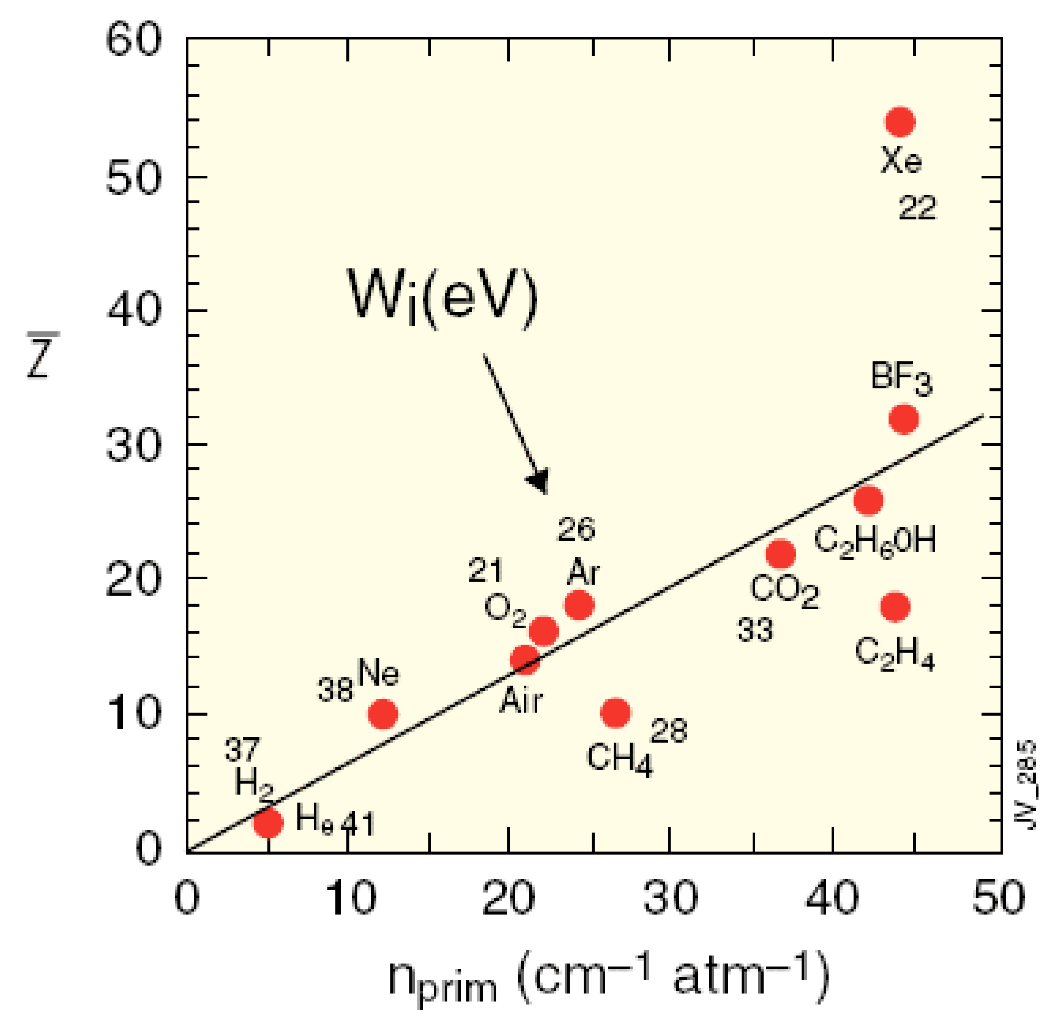

Number of primary electron/ion pairs in frequently used gases.

3. Primary Ionization in Gases

The actual number m of primary electron/ion pairs is Poisson distributed.

$$P(m) = \frac{\bar{n}^m e^{-\bar{n}}}{m!}$$

, where the average number of electron/ion pairs is $\bar{n} = \frac{L}{\lambda} = LN\sigma_i$

Detection efficiency ε: Depends on the minimum number of measurable electron/ion pairs

Example: m > 0 $\epsilon = 1 - P(0) = 1 - e^{-\bar{n}}$

For thin detector layers the efficiency can be significantly smaller then 1.
Example: 1 mm of Ar ; $\bar{n} = 2.5 \rightarrow \epsilon = 0.92$

Considering: Electronic noise in amplifier is typically 1000 e^- (ENC):

Conclusion: signal amplification in gas is needed!

3. Diffusion in Gases

Electrons and ions, produced by the ionization process, loose their energy by multiple collisions and thermalize with the temperature of the gas.

At room temperature: ε = (3/2) kT ≈ 0.04 eV

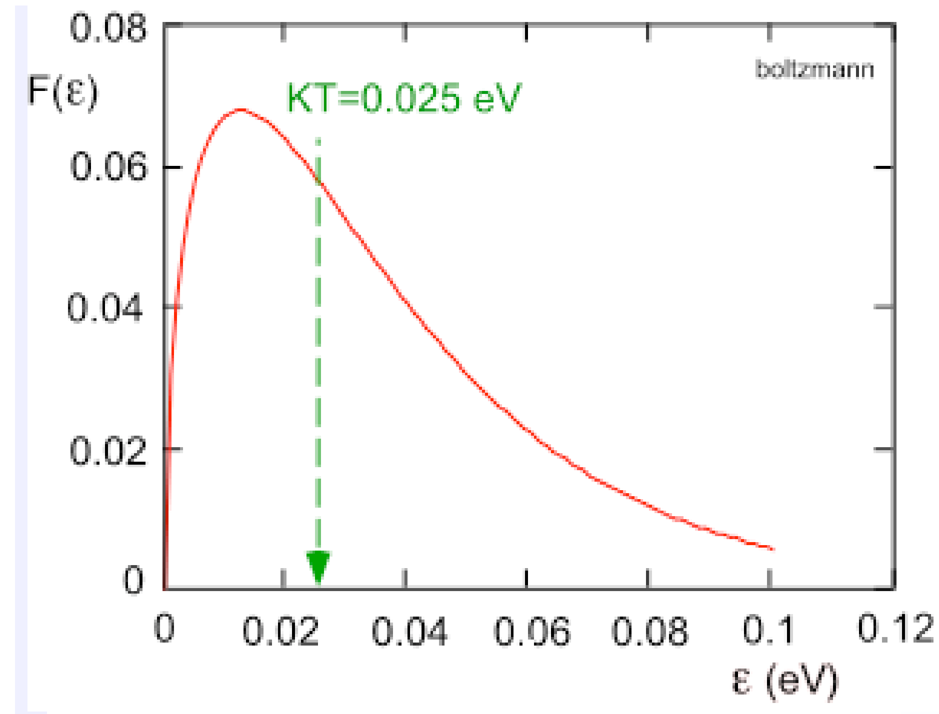

The energy distribution follows a Maxwell-Boltzmann-Distribution

$$F(\epsilon) = const \cdot \sqrt{\epsilon}\ \exp(-\epsilon/kT)$$

Due to multiple collisions (diffusion) there is a statistical distribution of charge, which is found in the length interval dx at distance x at a time t according to :

$$\frac{dN}{N} = \frac{1}{\sqrt{4\pi Dt}} \exp(-\frac{x^2}{4Dt}) dx$$

Linear diffusion: $\sigma_x = \sqrt{2Dt}$

Volume diffusion: $\sigma_{vol} = \sqrt{3}\ \sigma_x = \sqrt{6Dt}$

Average mean free path in diffusion: $\lambda = \frac{1}{N\sigma(\epsilon)}$

3. Drift and Diffusion in Gases

Average mean free path in diffusion:

$$\lambda = \frac{1}{N\sigma(\epsilon)}$$

where $\sigma(\varepsilon)$ is energy dependent collision cross section

$N = (N_A / A)\ \rho$: number of molecules per unit volume.

If charge carriers are in an electric field the ordered drift due to the E-field is superimposed by the statistical disordered movement due to diffusion.
The **drift velocity** of the charge carriers inside the gas can be defined as:

$$\vec{v}_{drift} = \mu(E)\ \vec{E}\ \frac{p_0}{p}$$

$\mu(E)$	energy dependent charge-carrier mobility
$\vec{E}$	electric field
p/p_0	pressure normalized to standard pressure

Note that the drift velocity scales with E/p (if μ is constant).

from L.Ropelewski

E=0 thermal diffusion $\langle v \rangle_t = 0$

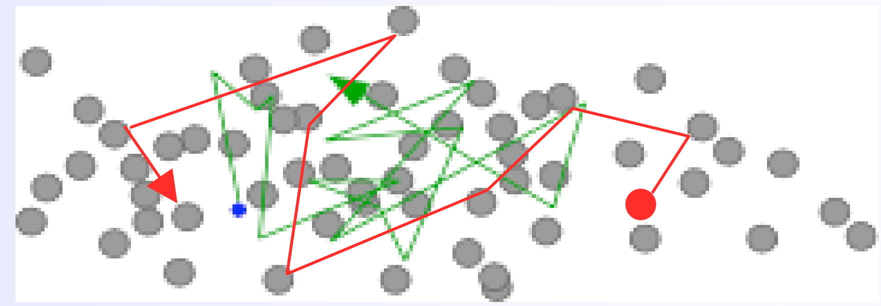

E>0 charge transport and diffusion $\langle v \rangle_t = v_D$

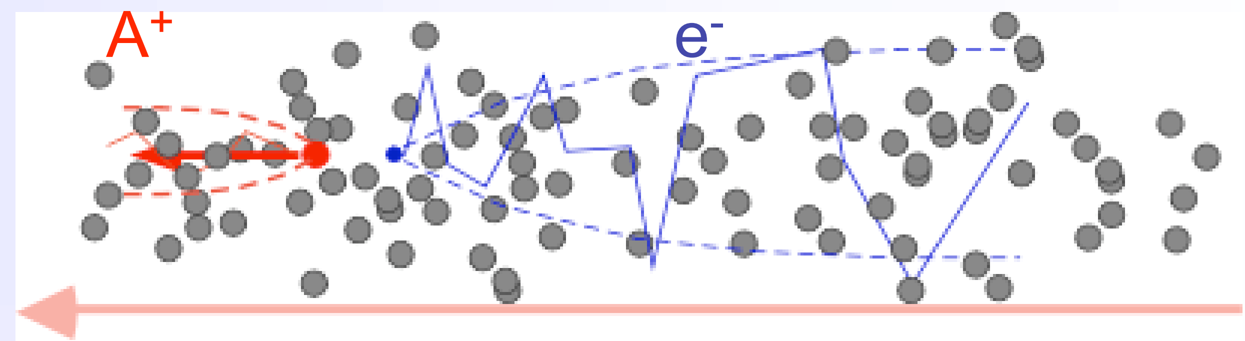

Electron swarm drift

Drift velocity

Diffusion

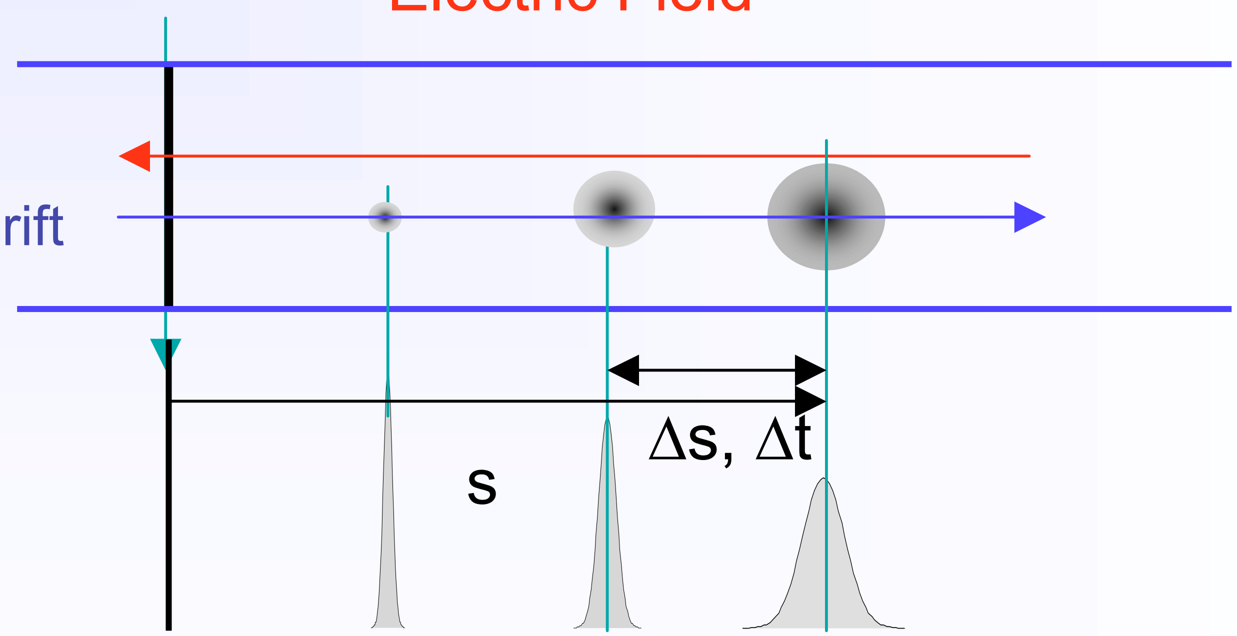

$$v_D = \frac{\Delta s}{\Delta t}$$

$$\sigma_x = \sqrt{2Dt} = \sqrt{2D\frac{s}{v_D}}$$

3. Lorentz Angle in Magnetic Fields

Lorentz angle (deflection angle of drift electrons due to magnetic field)

$$\tan\alpha = v_{drift}\,\frac{B}{E}$$

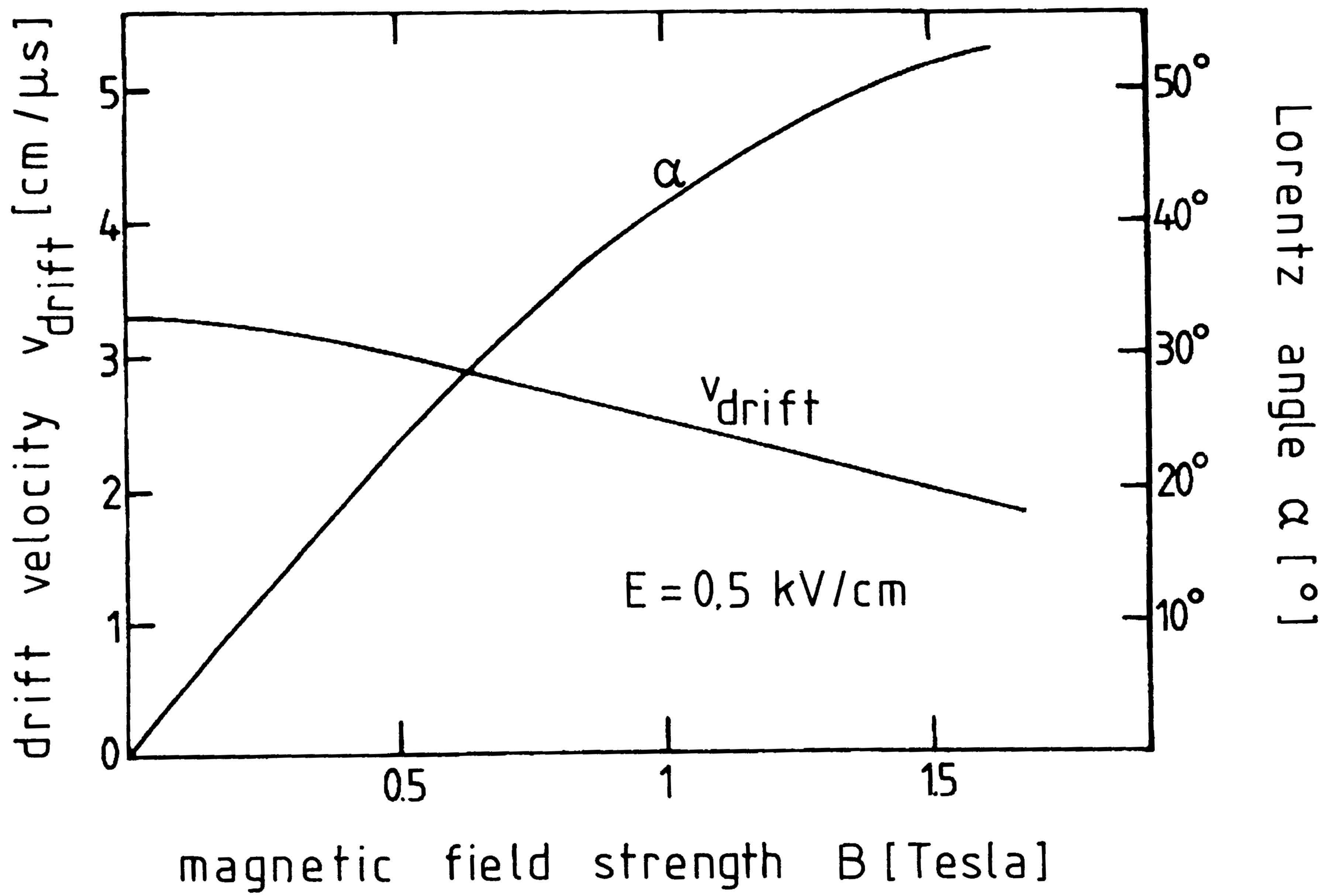

Fig. 1.21. Dependence of the electron drift velocity $\vec{v}_{\mathrm{drift}}$ and the Lorentz angle α on the magnetic field for low electric field strengths (500 V/cm) in a gas mixture of argon (67.2 %), isobutane (30.3 %) and methylal (2.5 %) [51, 95].

4. History of Tracking Detectors: Cloud Chamber (not shown)

Fig. 43. Radiation Laboratory, Berkeley, Cal.

Fast electron in a magnetic field at the Bevatron, 1940

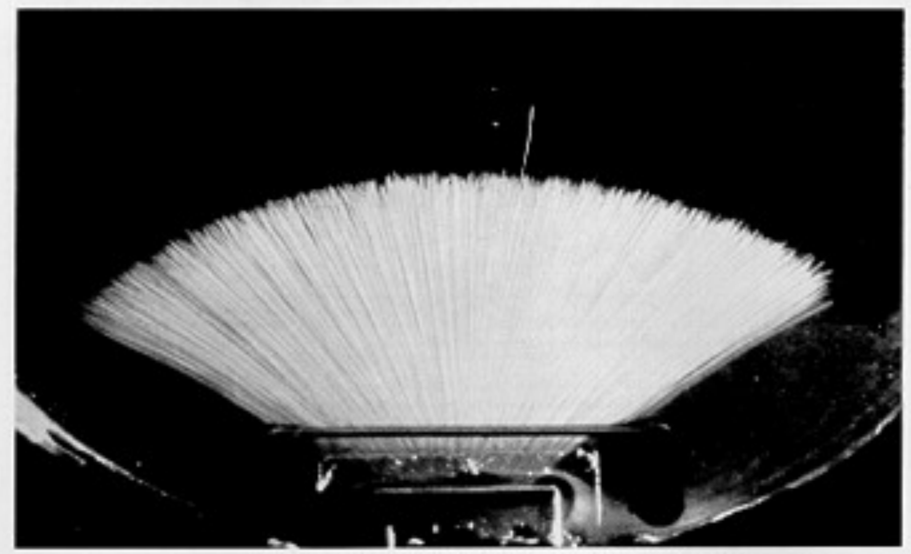

Fig. 13. K. Philipp, Naturwiss. 14, 1203 (1926).

α-particles in air.

In cloud chambers a charged particle causes condensation of a supersaturated gas.

The picture (left) shows and electron with 16.9 MeV initial energy.

It spirals about 36 times in the magnetic field.

Nobel prizes related to cloud chamber development:
C. T. R. Wilson, 1927
P.M.S. Blackett, 1948 (triggered chambers)

4. History of Tracking Detectors: Nuclear Emulsion (not shown)

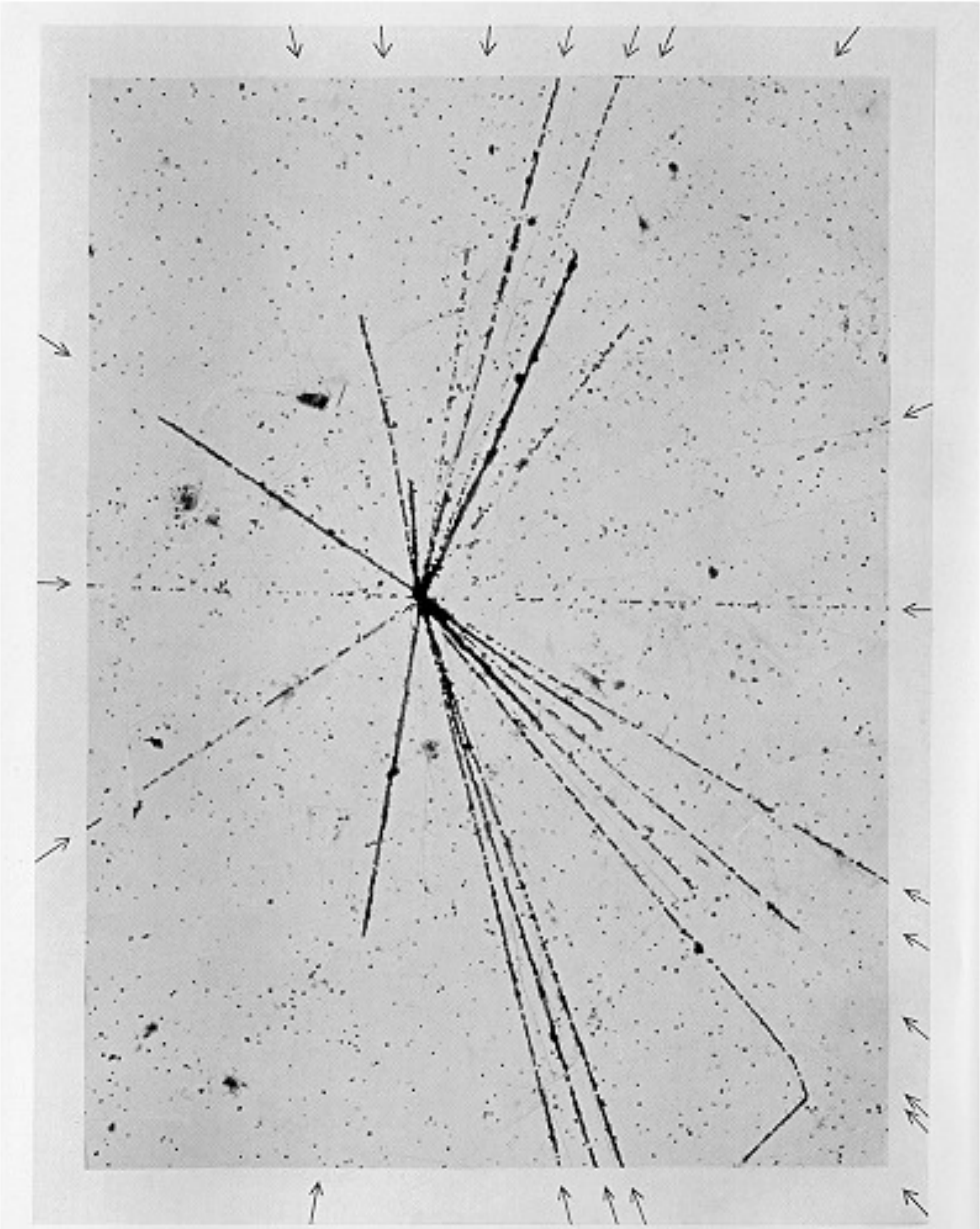

'EXPLOSIVE' DISINTEGRATION OF A NUCLEUS

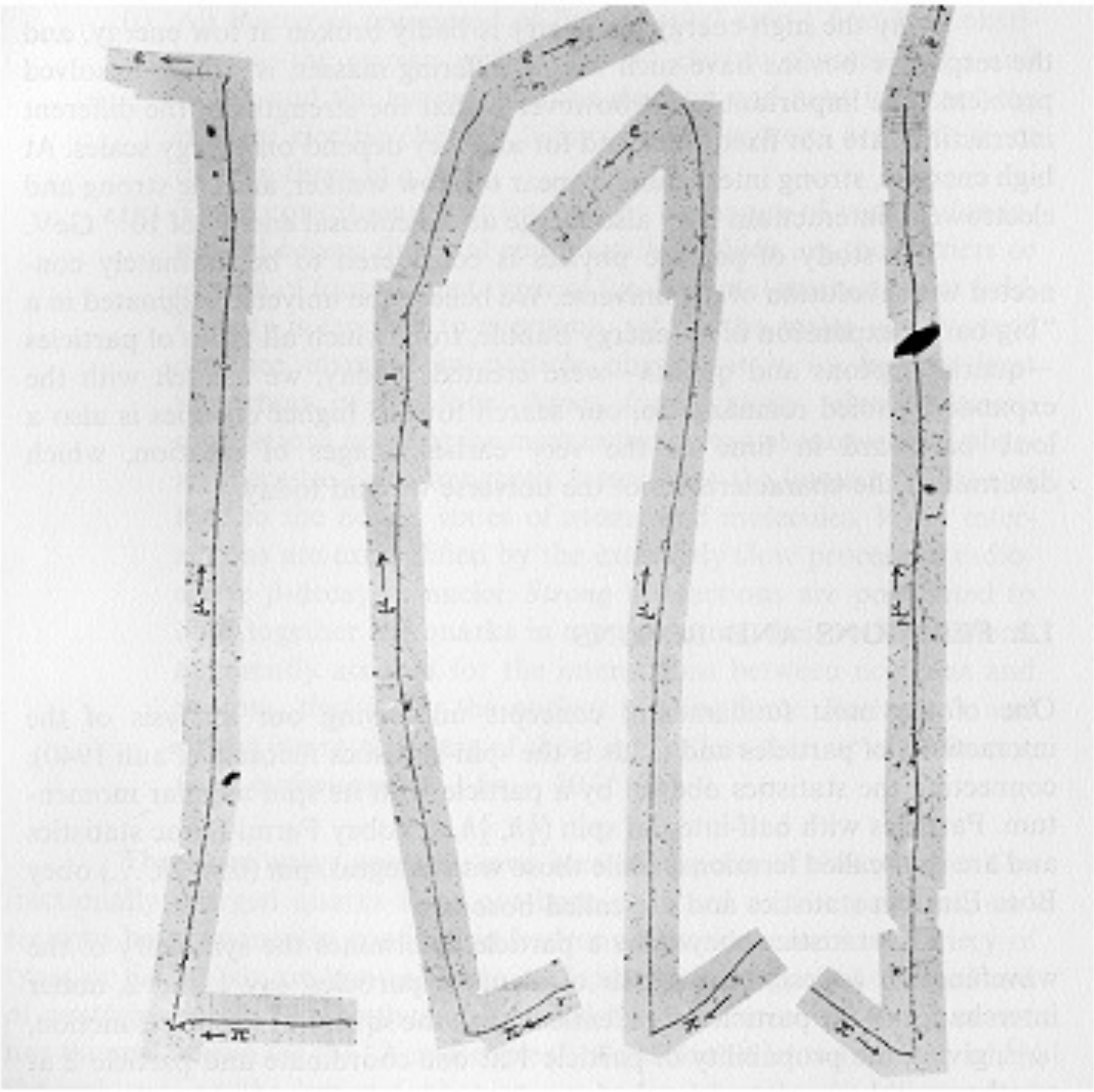

Discovery of muon and pion

Emulsion detectors are still used today: Opera experiment at Gran Sasso for the identification of tau decays.

4. Bubble Chambers

(not shown)

Cloud chamber: supersaturating a gas with a vapor.
Bubble chamber: superheated liquid. Invented by Donald A. Glazer, Nobel Prize 1960.
A particle depositing energy along it's path makes the liquid boil and forms bubbles.

The 80-inch Bubble Chamber

BNL, First Pictures 1963, 0.03s cycle

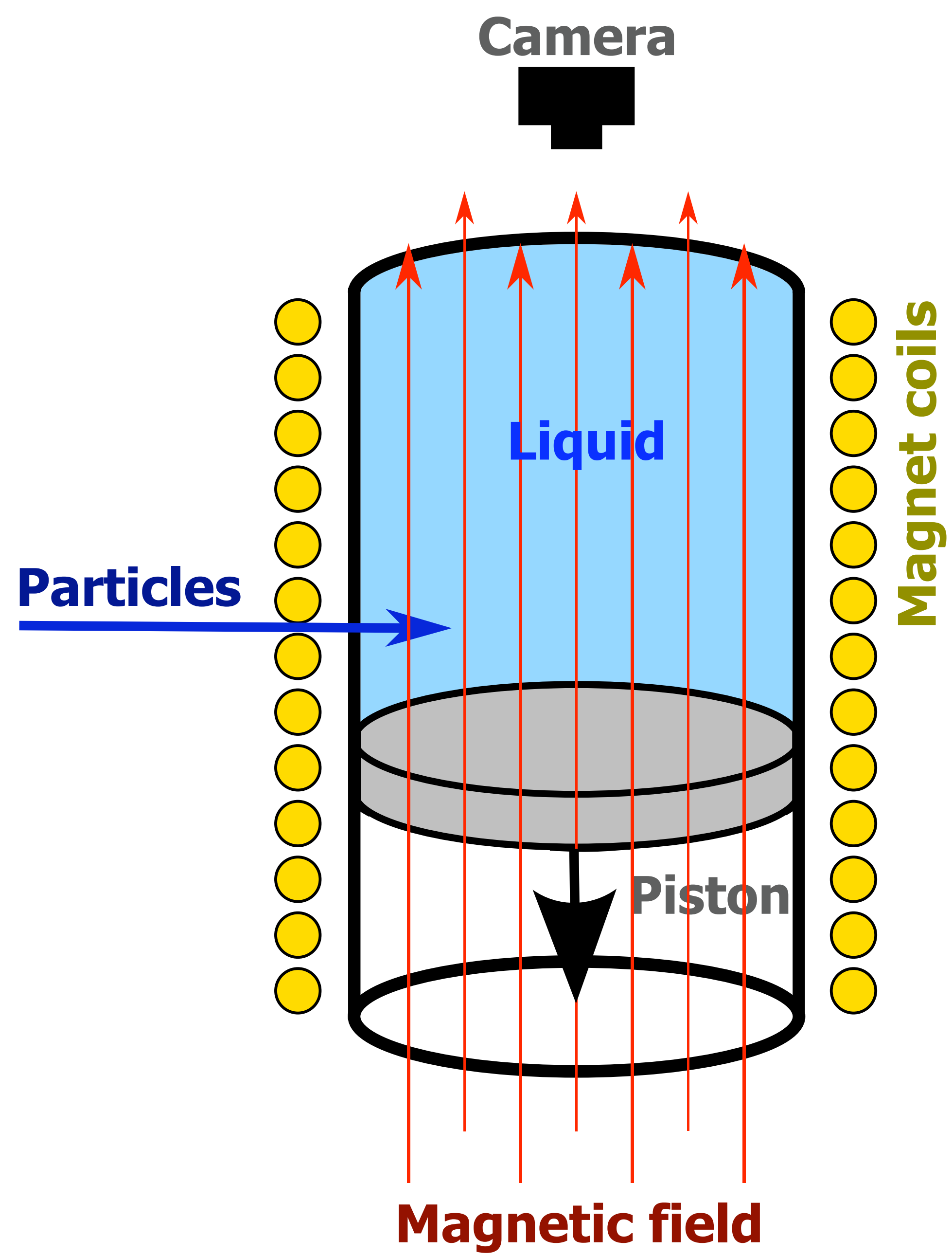

4. Bubble Chamber : BEBC

(not shown)

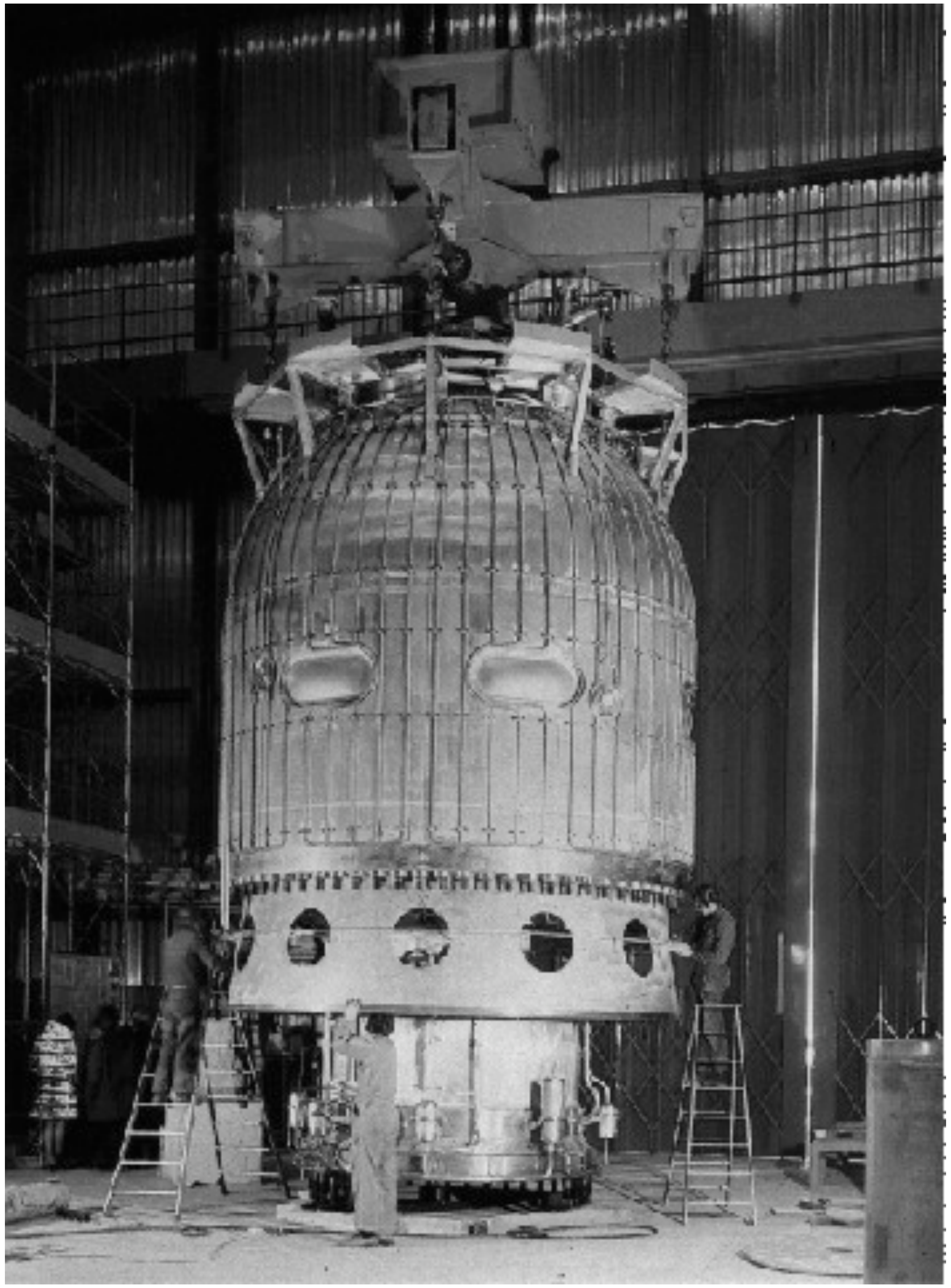

3.7 meter hydrogen bubble chamber at CERN, equipped with the largest superconducting magnet in the world at that time.

During its working life from 1973 to 1984, the "Big European Bubble Chamber" (BEBC) took over 6 million photographs.

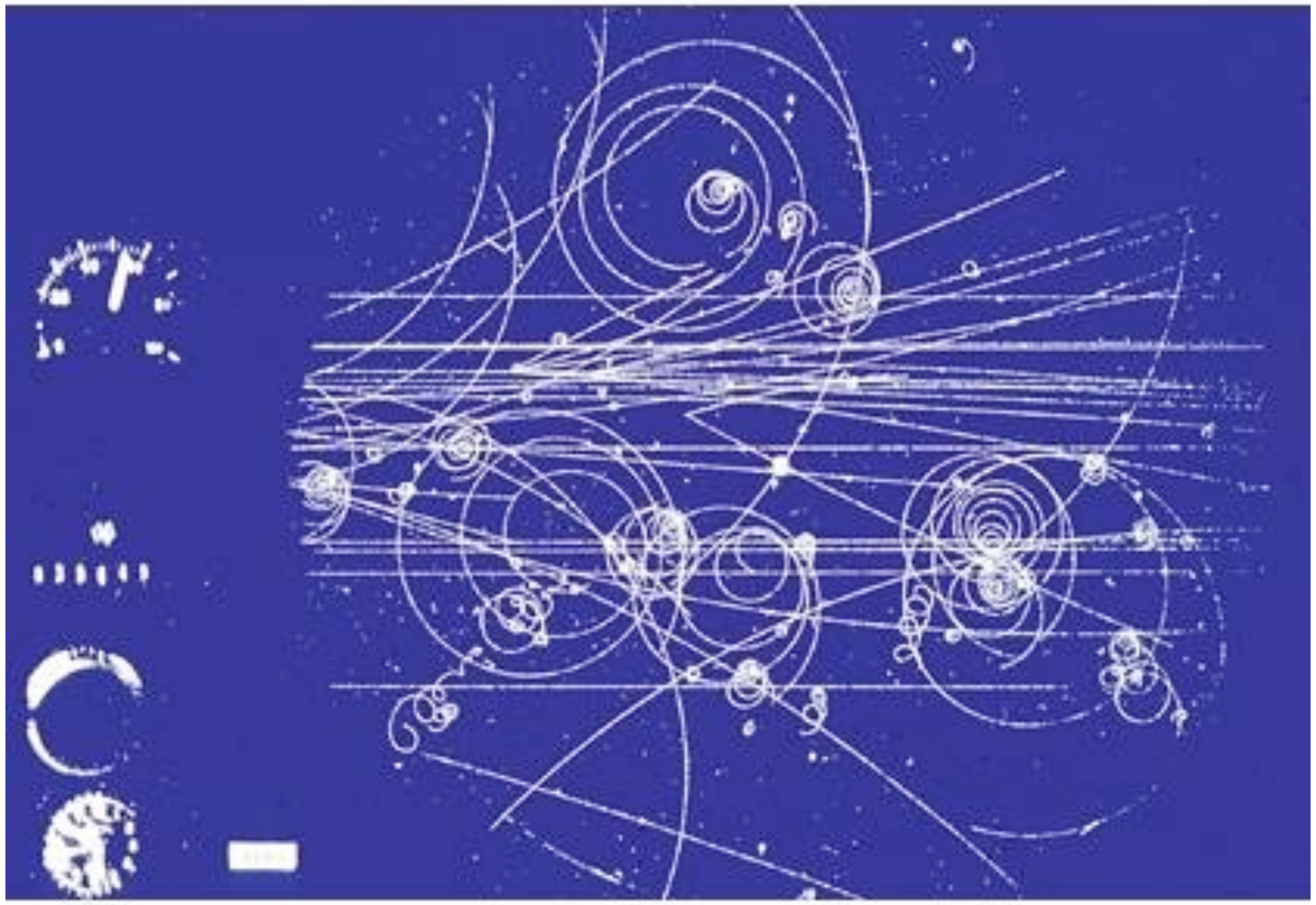

Can be seen outside the Microcosm Exhibition

4. Bubble Chambers

(not shown)

The excellent position (5μm) resolution and the fact that target and detecting volume are the same (H chambers) makes the Bubble chamber almost unbeatable for reconstruction of complex decay modes.

The drawback of the bubble chamber is the low rate capability (a few tens/ second). E.g. LHC 10^9 collisions/s.

The fact that it cannot be triggered selectively means that every interaction must be photographed.

Analyzing the millions of images by 'operators' was a quite laborious task.

That's why electronics detectors took over in the 70ties.

4. Spark Chamber

(not shown)

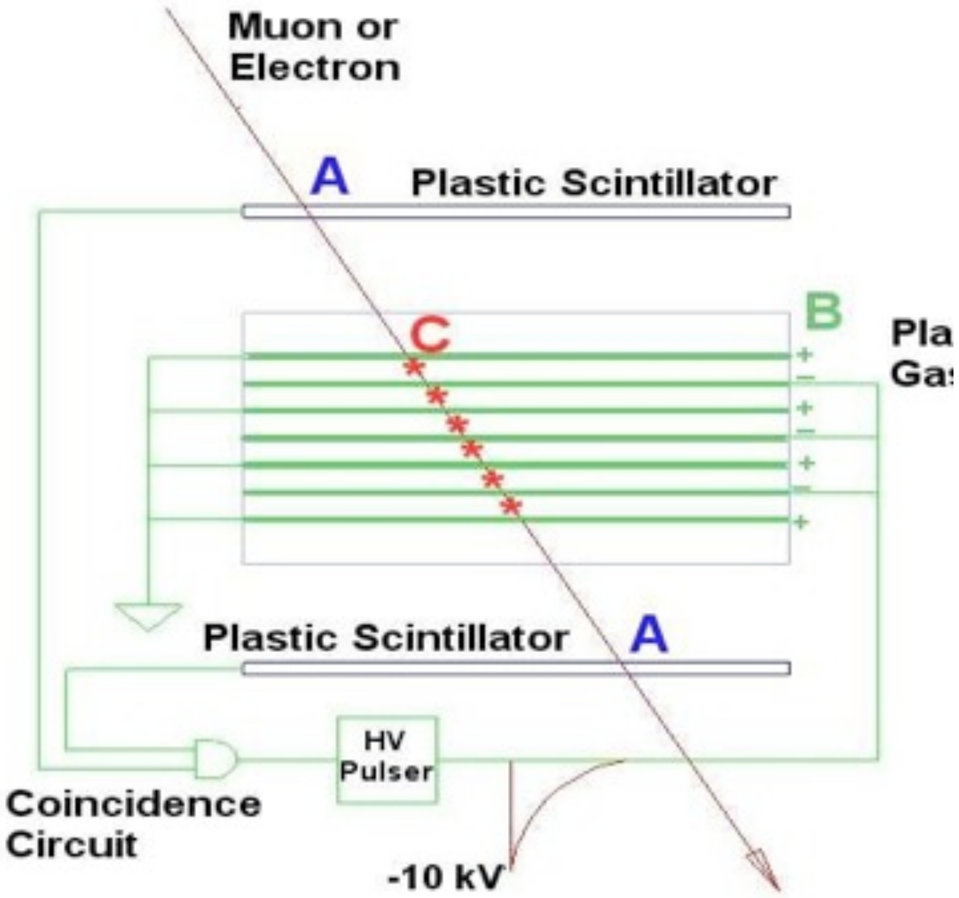

The Spark Chamber was developed in the early 60ies.

Schwartz, Steinberger and Lederman used it in discovery of the muon neutrino

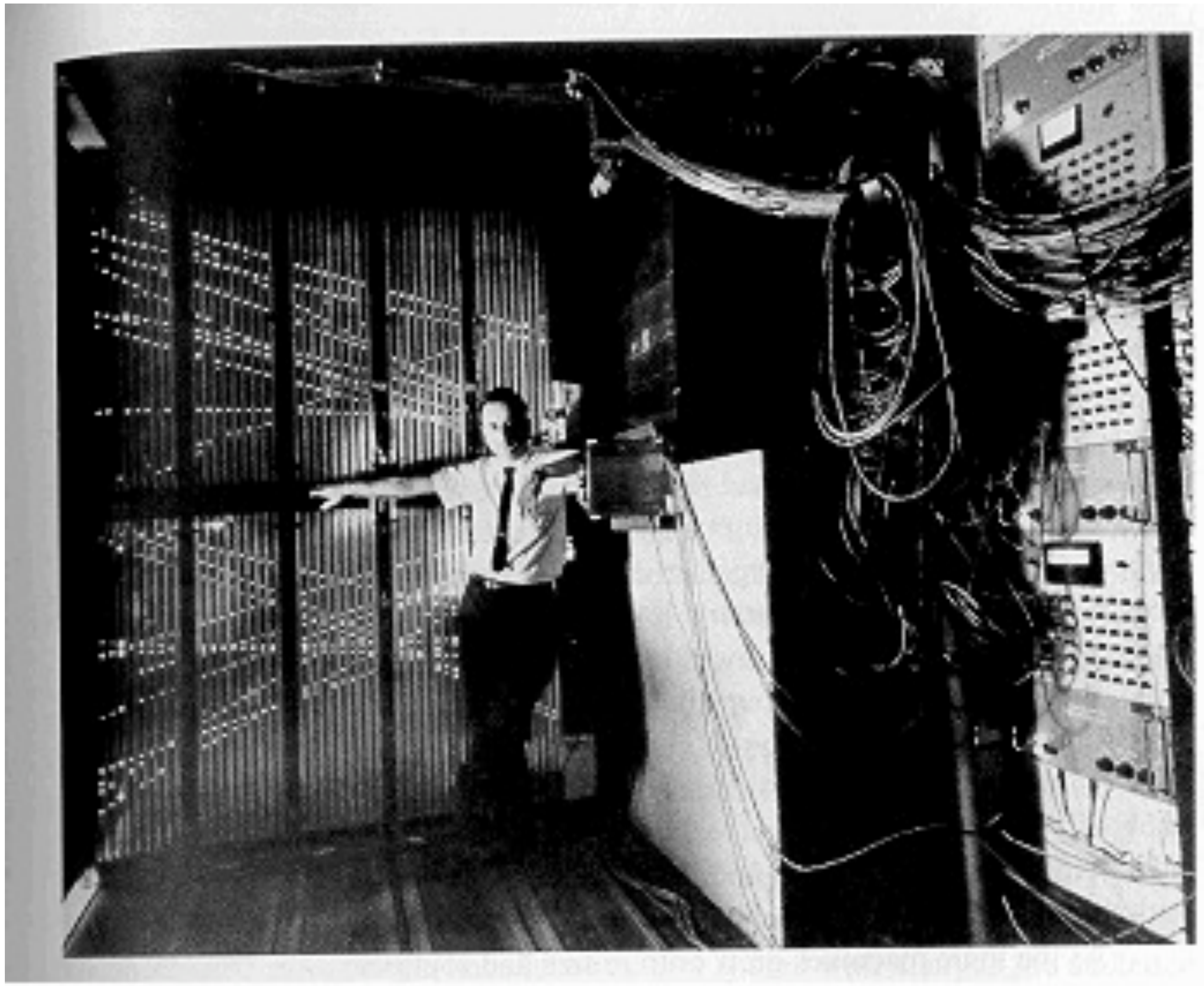

A charged particle traverses the detector and leaves an ionization trail.

The scintillators trigger an HV pulse between the metal plates and sparks form in the place where the ionization took place.

4. History: Multi Wire Proportional Chambers (not shown)

Tube, Geiger- Müller, 1928

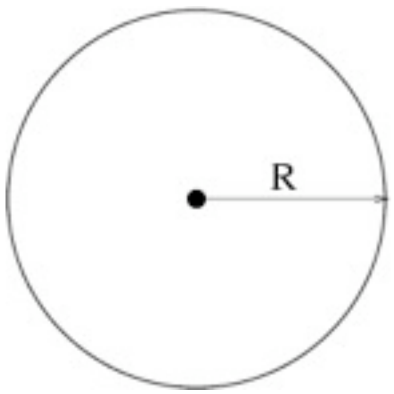

Multi Wire Geometry, in H. Friedmann 1949

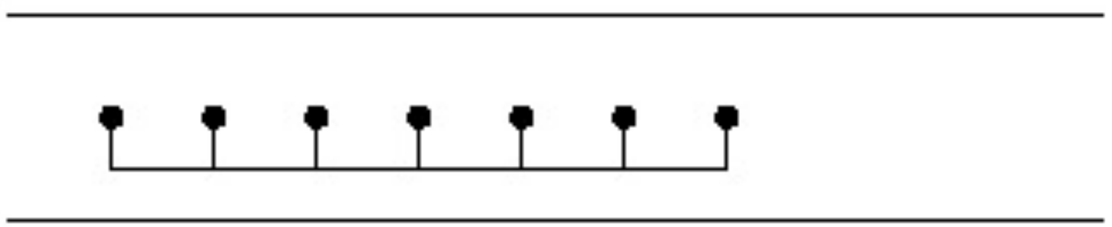

G. Charpak 1968, Multi Wire Proportional Chamber, readout of individual wires and proportional mode working point.

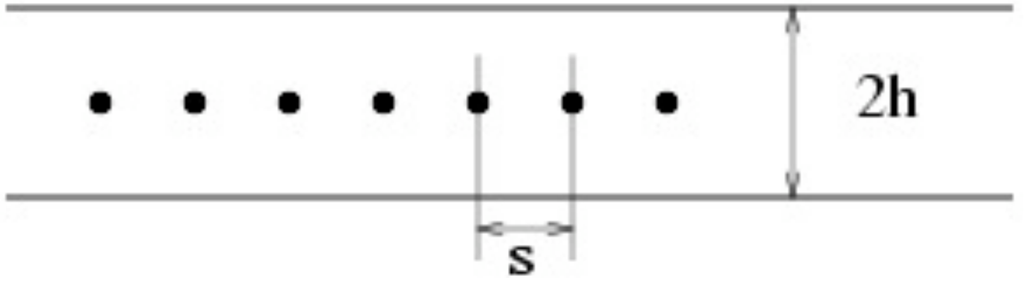

5. Proportional Chamber : Single Wire

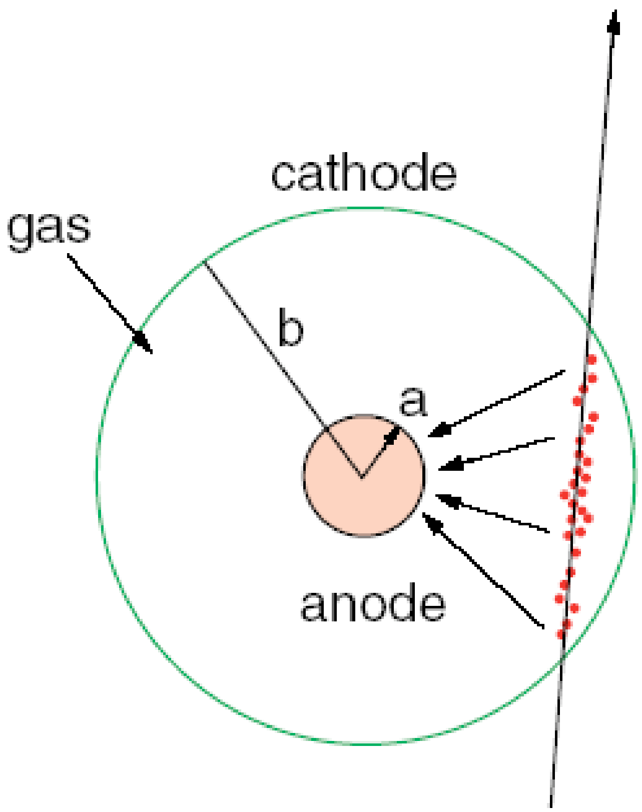

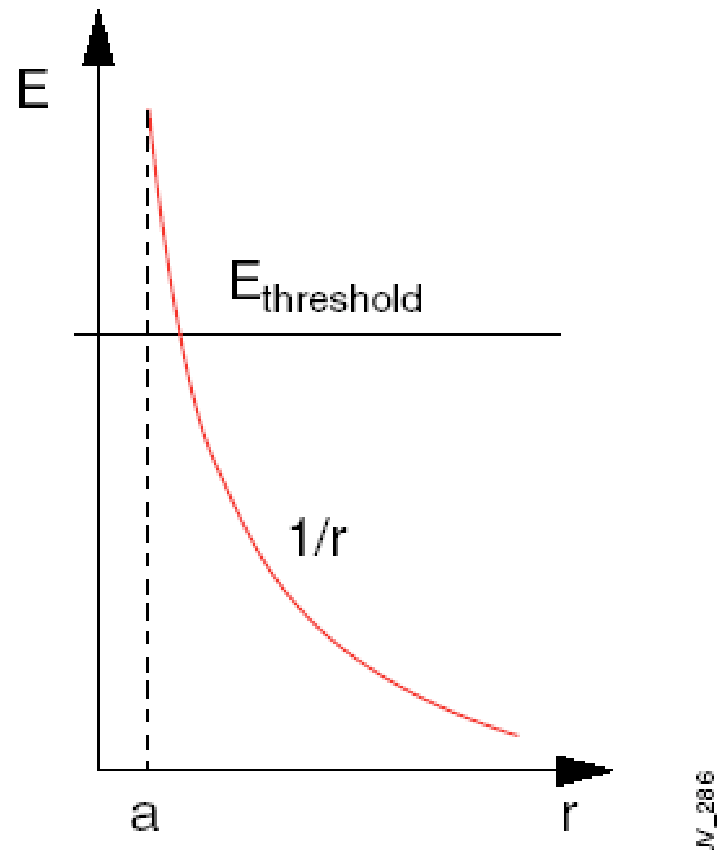

Electrons produced by ionization drift to the anode wire.

Avalanche:

- Close to the wire (∅ about few tens of µm) the E-field is very large (> 10 kV/cm).
- Between collisions electrons gain enough energy to ionize gas.
- Exponential increase of number of electron/ion pairs (gas amplification)

$$n = n_0 \; e^{\alpha(E)x}$$

α is the first Townsend coefficient.

Electric field: $$E(r) = \frac{CV_0}{2\pi\epsilon_0} \frac{1}{r}$$

Potential: $$V(r) = \frac{CV_0}{2\pi\epsilon_0} \ln \frac{r}{a}$$

V_0 = voltage between anode-cathode

Capacitance per length $$C = \frac{2\pi\epsilon}{\ln(b/a)}$$

5. Single Wire Proportional Chamber

SWPC OPERATION MODE

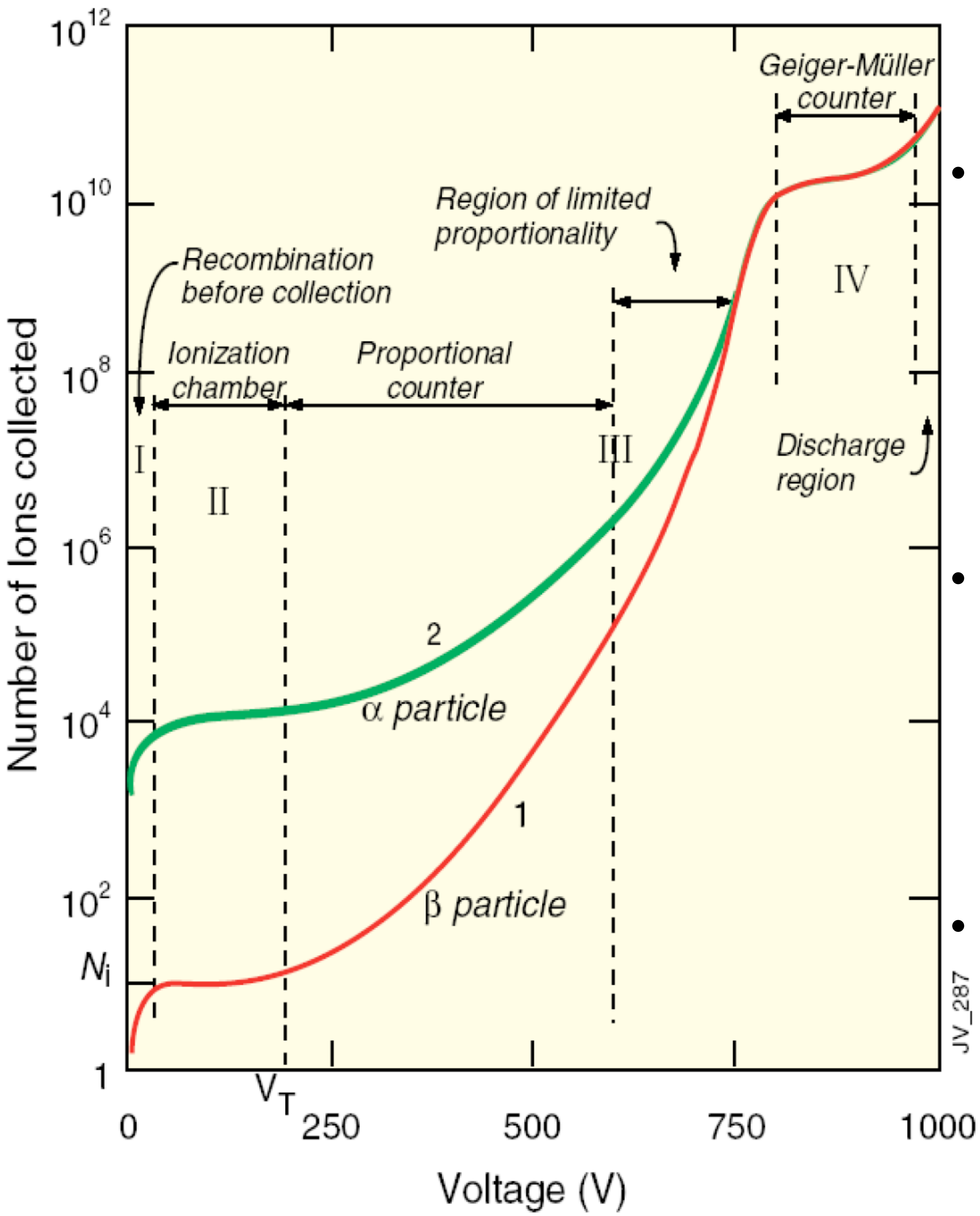

- ionization mode
  - full charge collection
  - no multiplication
  - gain ~ 1
- proportional mode
  - multiplication of ionization
  - signal proportional to ionization
  - measurement of dE/dx
  - secondary avalanches
  - have to be quenched;
  - gain ~ $10^4 – 10^5$
- limited proportional mode
  - (saturated, streamer)
  - strong photoemission
  - secondary avalanches
  - requires strong quenchers or pulsed HV; gain ~ 10^{10}
- Geiger mode
  - massive photoemission; full length of the anode wire affected;
  - discharge stopped byHV cut

5. Single Wire Proportional Chamber

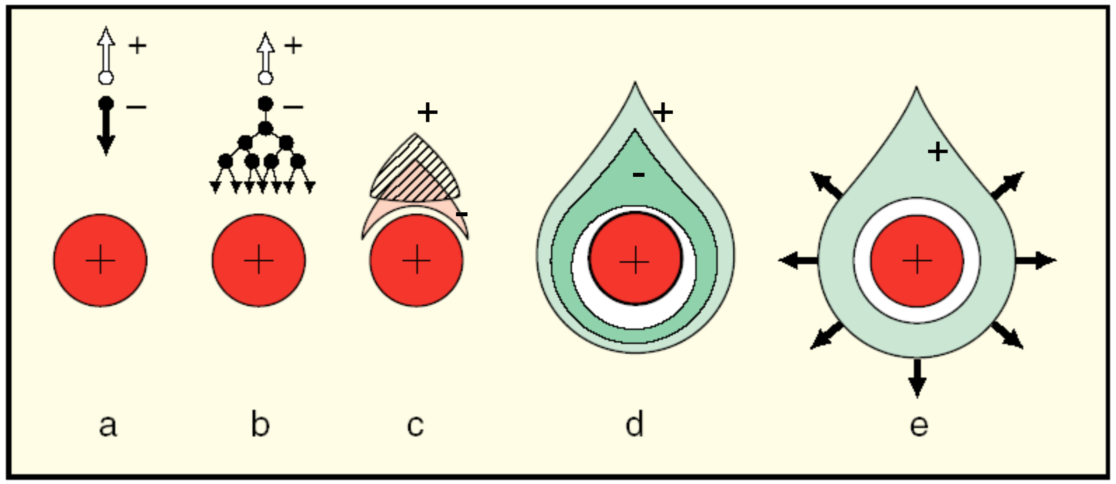

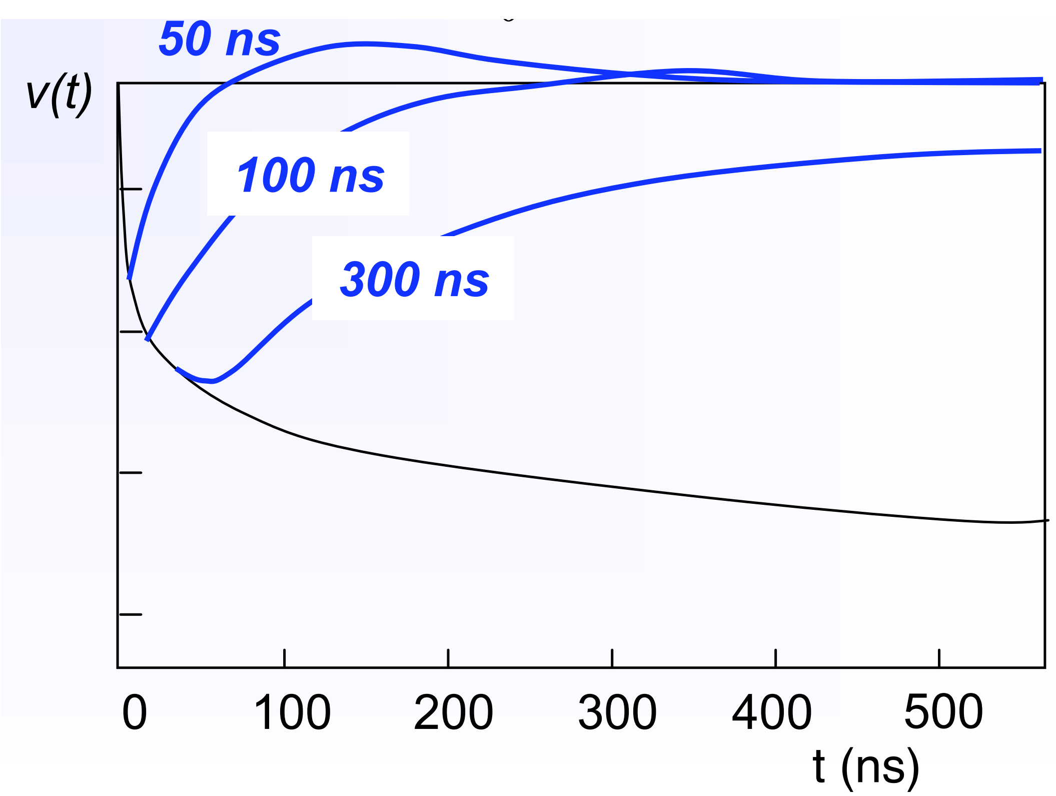

Time for ion signal is very long due to the long drift path.
Need to differentiate signal with time constant τ=RC.

Avalanche formation happens near the wire within time < 1 ns.

Signal induced on anode and cathode due to moving charges (electrons and ions).

Work to move charge q by dr:

$$dW = lCV_0\ dV = q\frac{dV(r)}{dr}dr$$

Induced voltage: $$dV = \frac{q}{lCV_0}\frac{dV(r)}{dr}dr$$

Total voltage induced in a cylindrical tube (a < r < b) for gas multiplication at distance d from anode, from electrons (V^-) and ions (V^+):

$$V^- = \frac{-q}{lCV_0}\int_{a+d}^{a}\frac{dV(r)}{dr}dr = -\frac{q}{2\pi\epsilon l}\ln\left(\frac{a+d}{a}\right)$$

$$V^+ = \frac{q}{lCV_0}\int_{a+d}^{b}\frac{dV(r)}{dr}dr = -\frac{q}{2\pi\epsilon l}\ln\left(\frac{b}{a+d}\right)$$

Ratio: $$\frac{V^-}{V^+} = \frac{\ln[(a+d)/a]}{\ln[b/(a+d)]} < 1\%$$

for
a=10 μm
b=10 mm
d=1 μm

5. Multi Wire Proportional Chamber (MWPC)

from L. Ropelewski

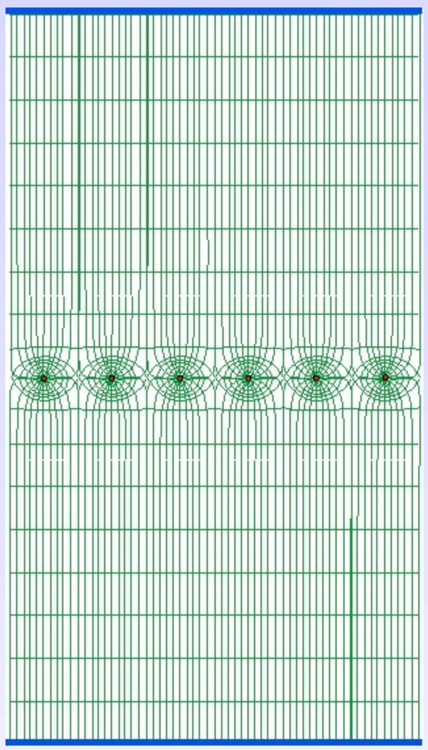

Simple idea to multiply SWPC cell : Nobel Prize 1992

First electronic device allowing high statistics experiments !!

Typical geometry

5mm, 1mm, 20 µm

Normally digital readout :

spatial resolution limited to

$$\sigma_x \approx \frac{d}{\sqrt{12}}$$

for d=1 mm
σ_x = 300 µm

$$\langle x^2 \rangle = \frac{\int_0^{d/2} x^2 dx}{\int_0^{d/2} dx} = \frac{2}{d} \frac{x^3}{3} \Big|_0^{d/2} = \frac{d^2}{12}$$

First large size MWPC

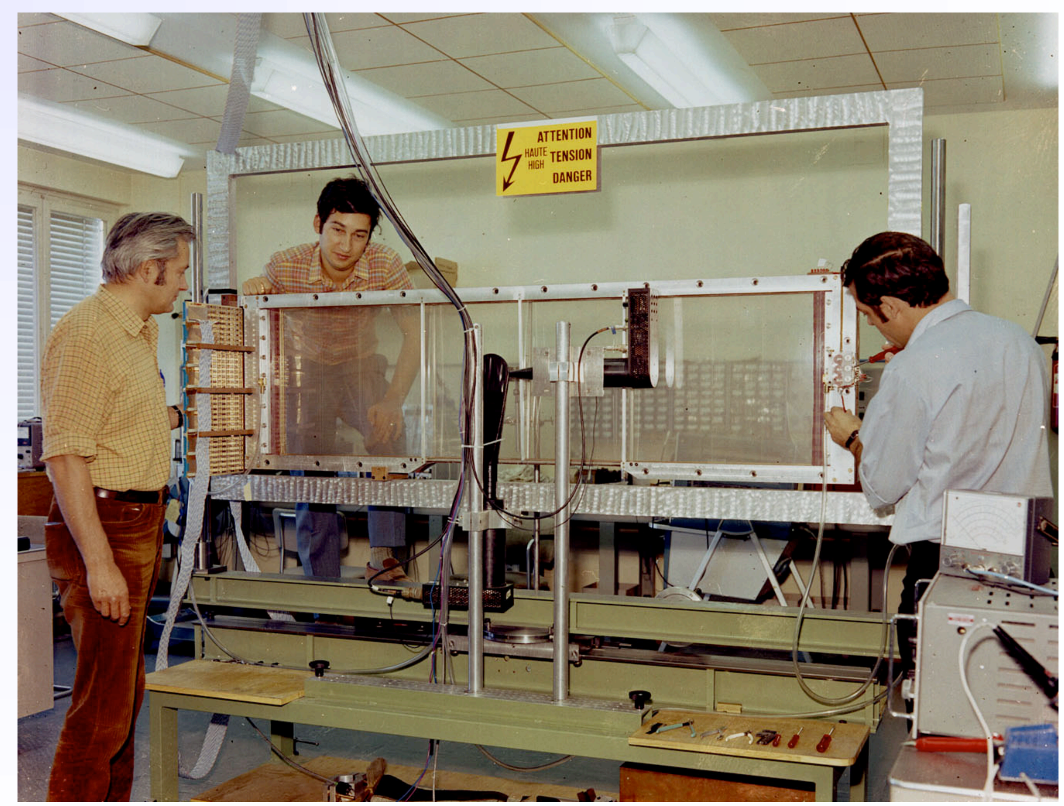

G. Charpak, F. Sauli and J.C. Santiard ,1970

5. MWPC: Two Dimensional Readout

Two coordinates (x,y) of the track hit can be determined from the position of the anode wire and the signal induced on the cathode strips (or wires).

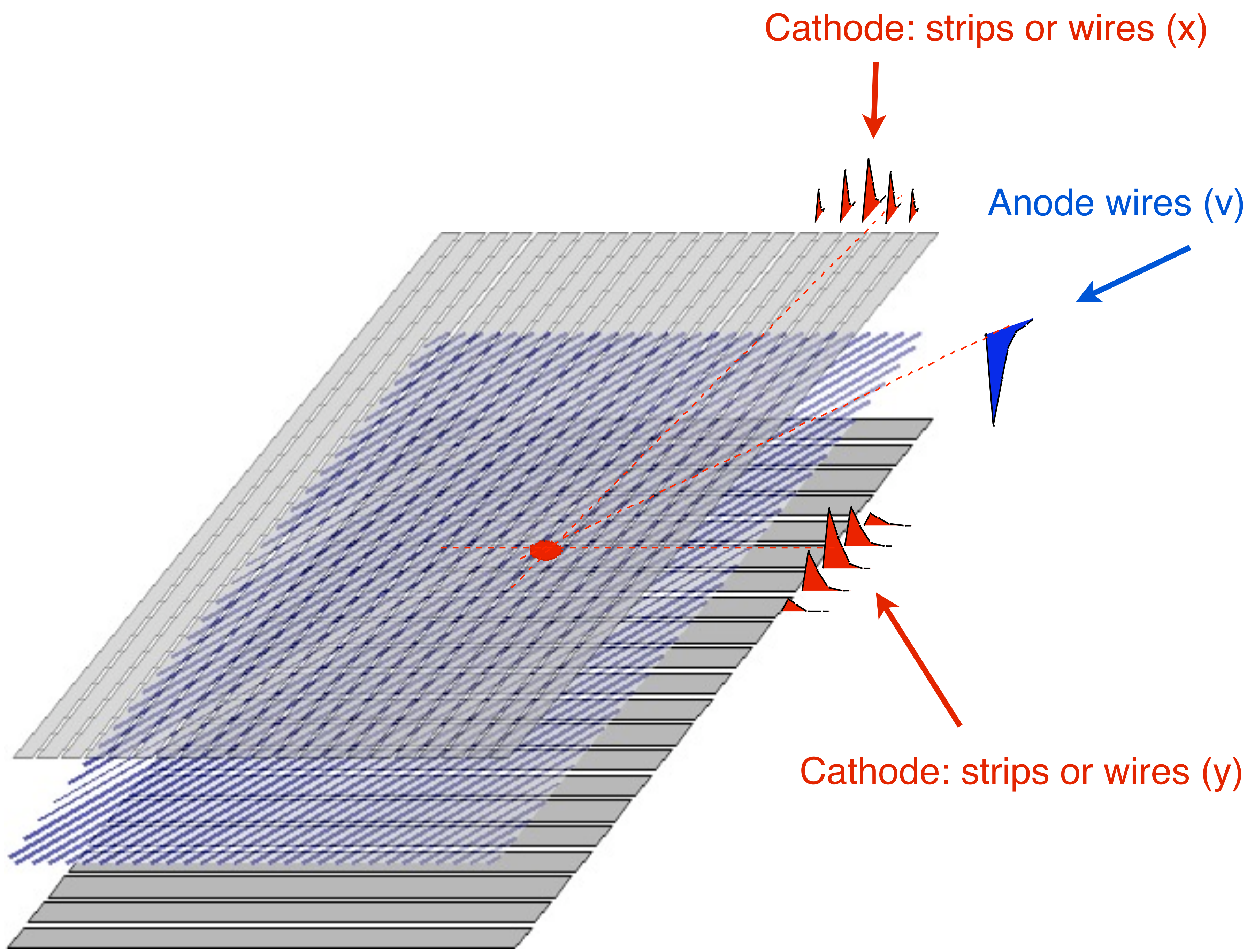

5. MWPC: Typical experimental set up

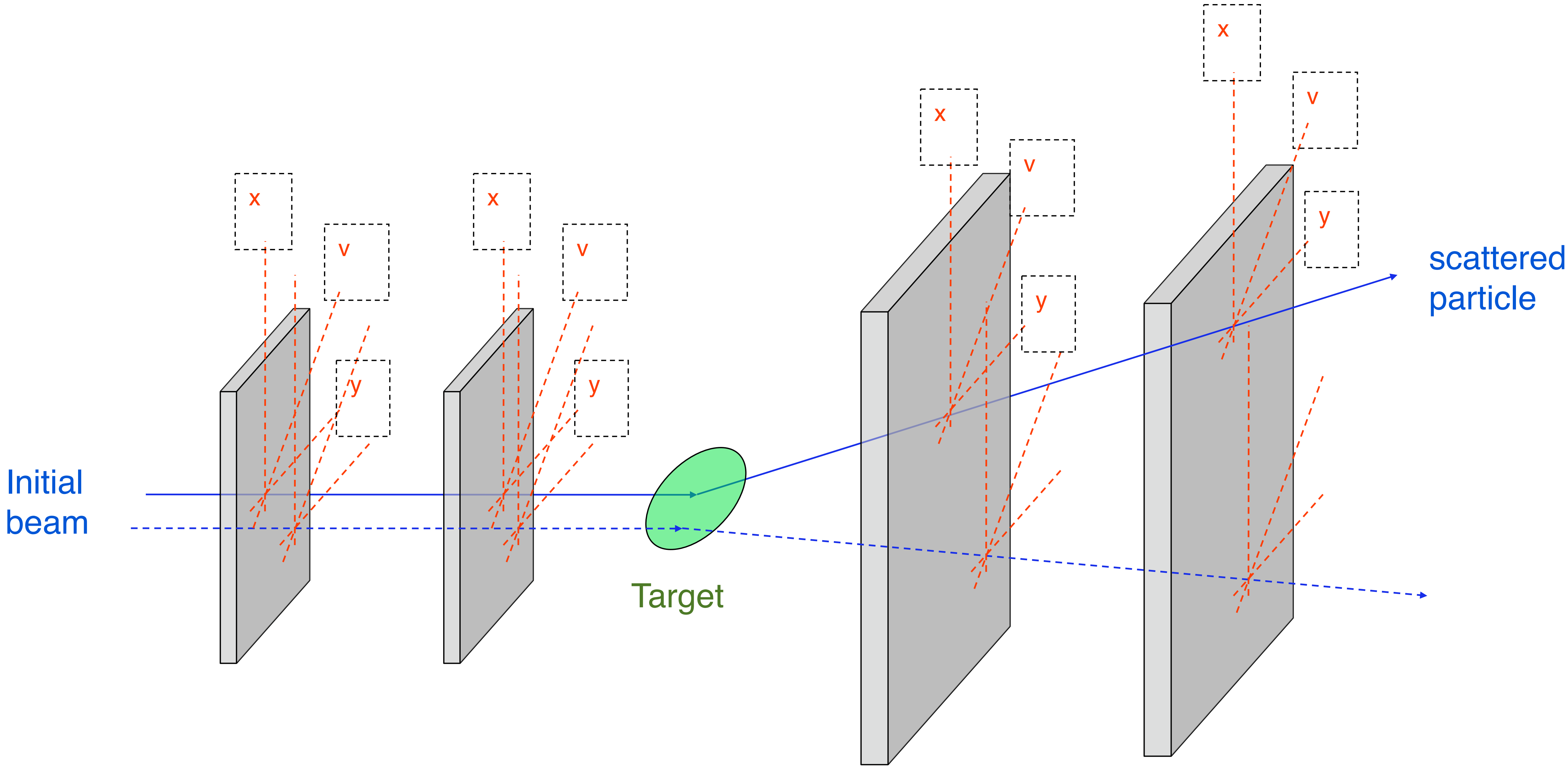

With this experimental set-up based on MWPC an event rate of about 100 000 Hz can be processed.
The position resolution in each layer is about 1 mm.

5. MWPC: Many Wire Planes

MWPC with many wire planes. 1985

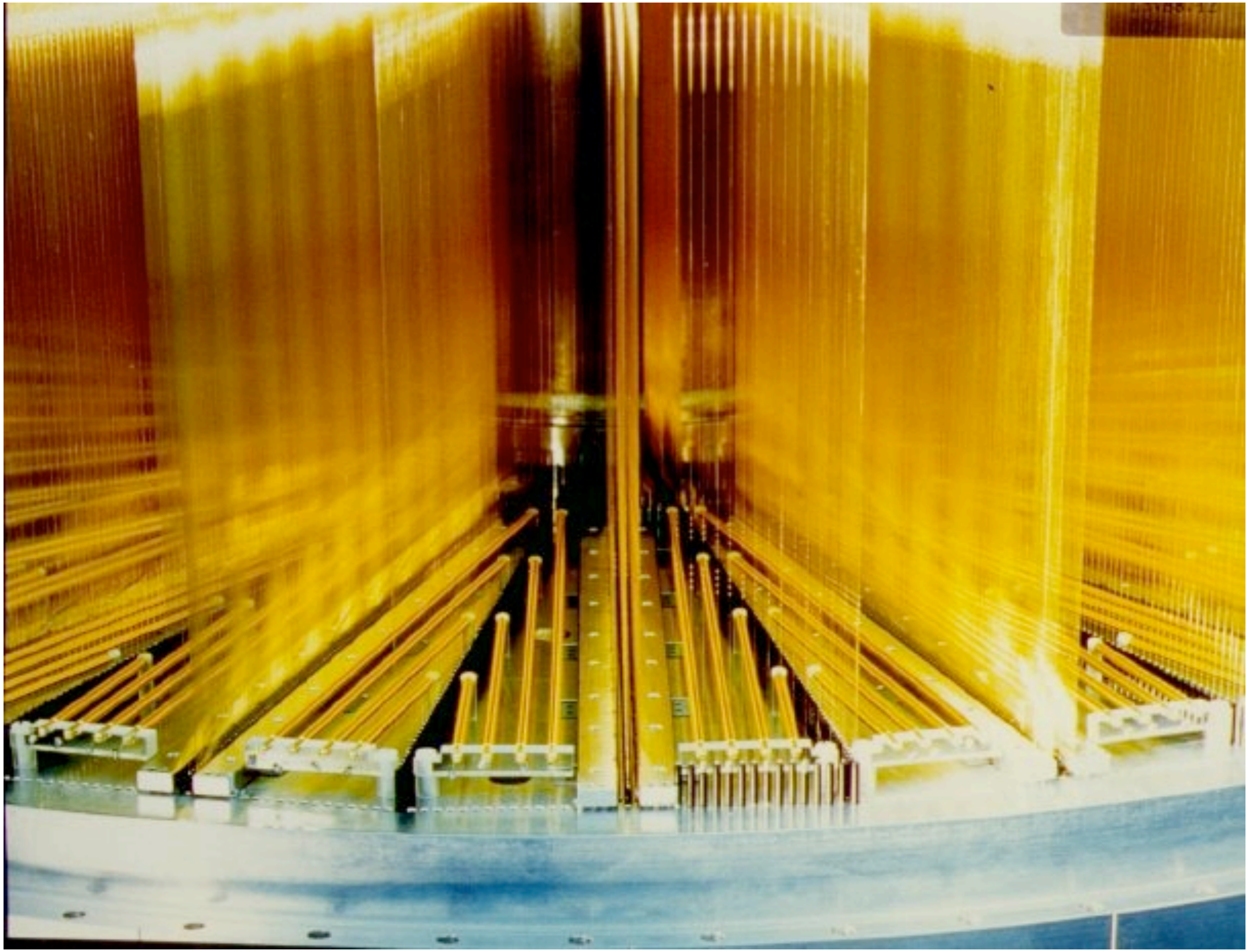

5. Cathode Strip Chamber

from L. Ropelewski

Precise measurement of the second coordinate by interpolation of the signal induced on pads.
Closely spaced wires makes CSC fast detector.

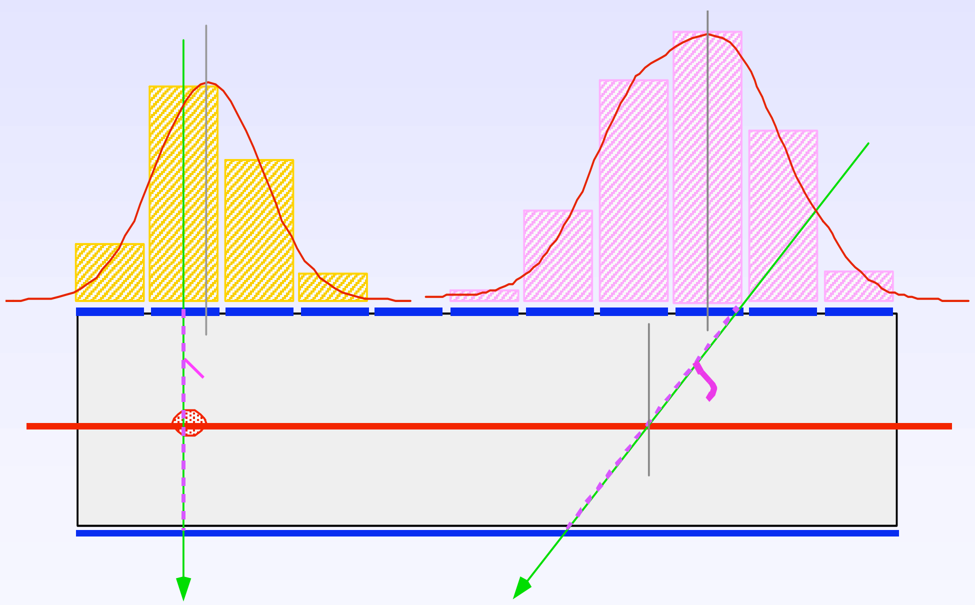

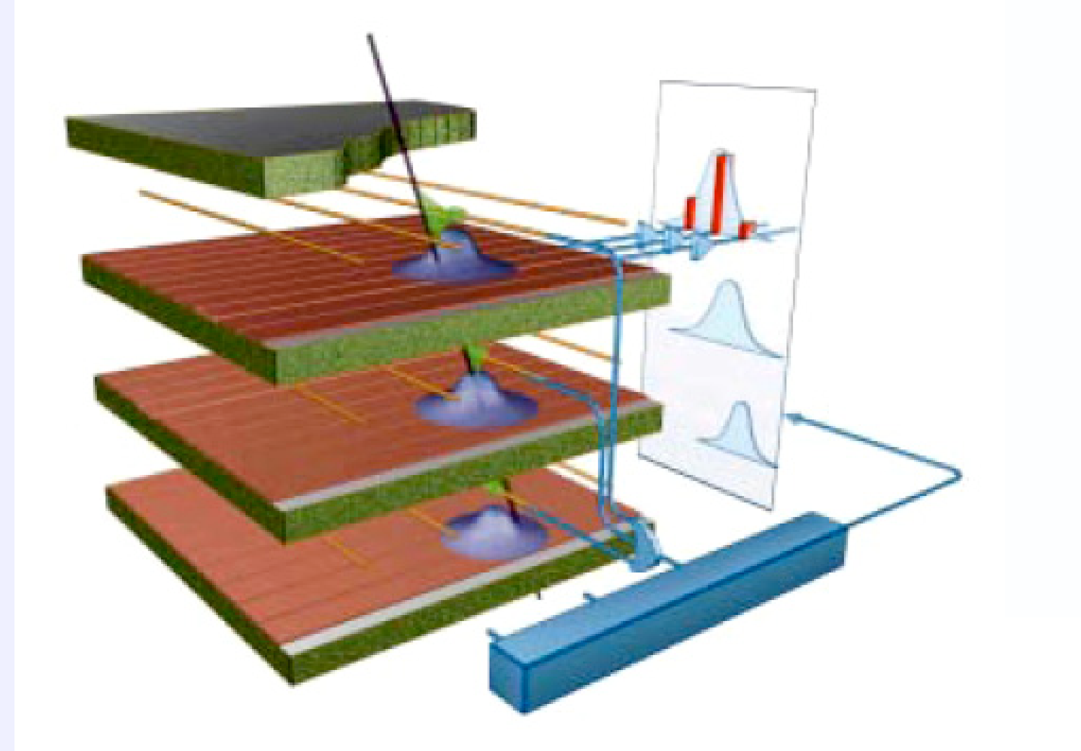

Center of gravity of induced signal method.

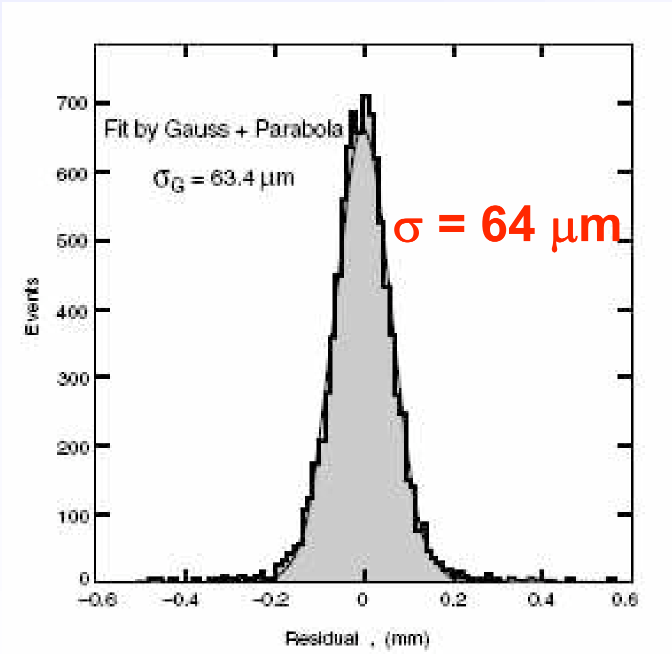

Space resolution

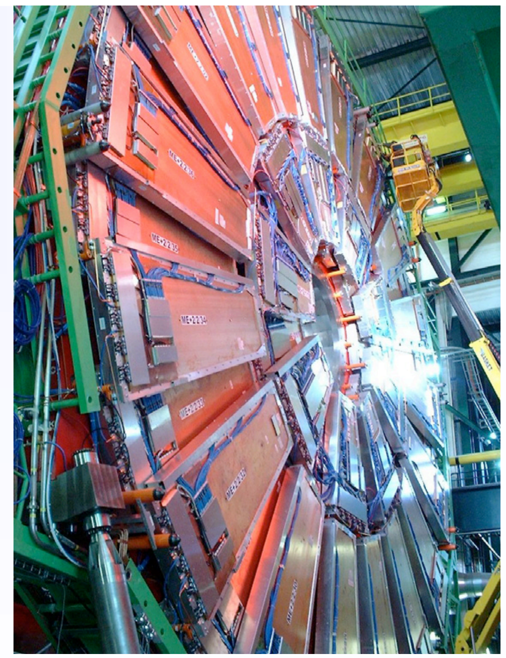

CMS

5. CMS Muon System

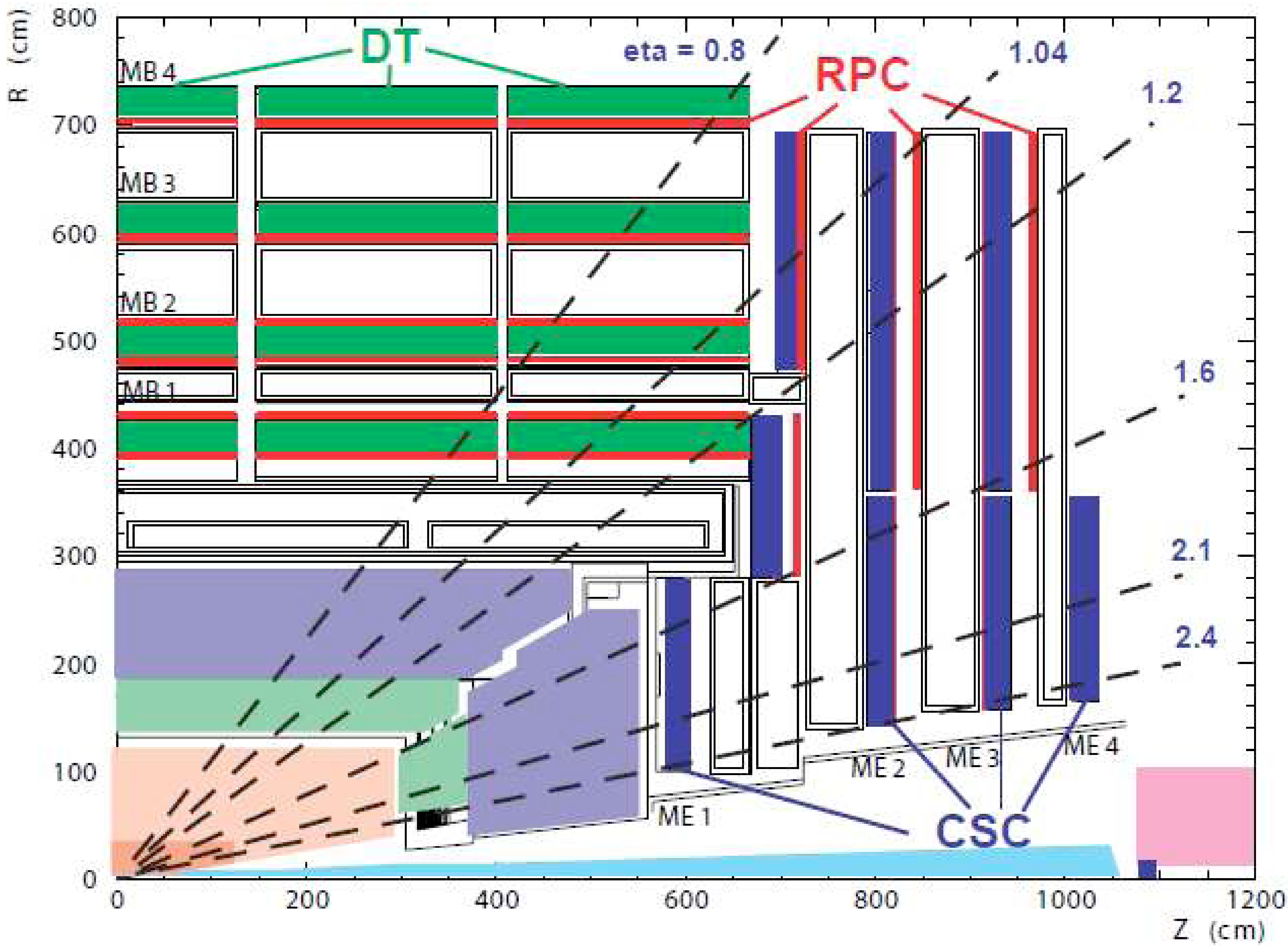

5. CMS Cathode Strip Chamber Occupancy

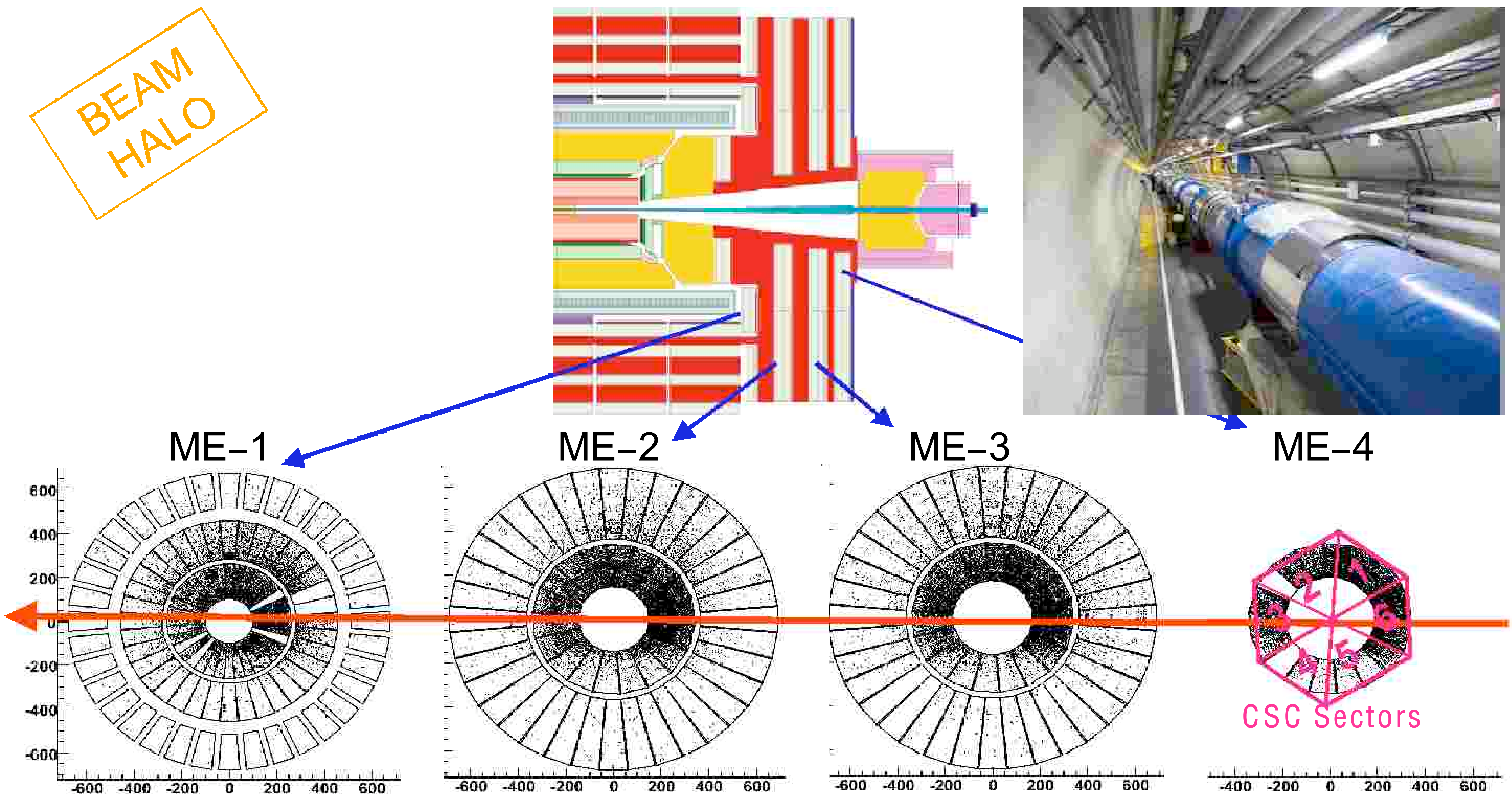

5. CMS Cathode Strip Efficiency

Cosmic Ray At Four Tesla

CRAFT

Average measured efficiencies for each station/ring.

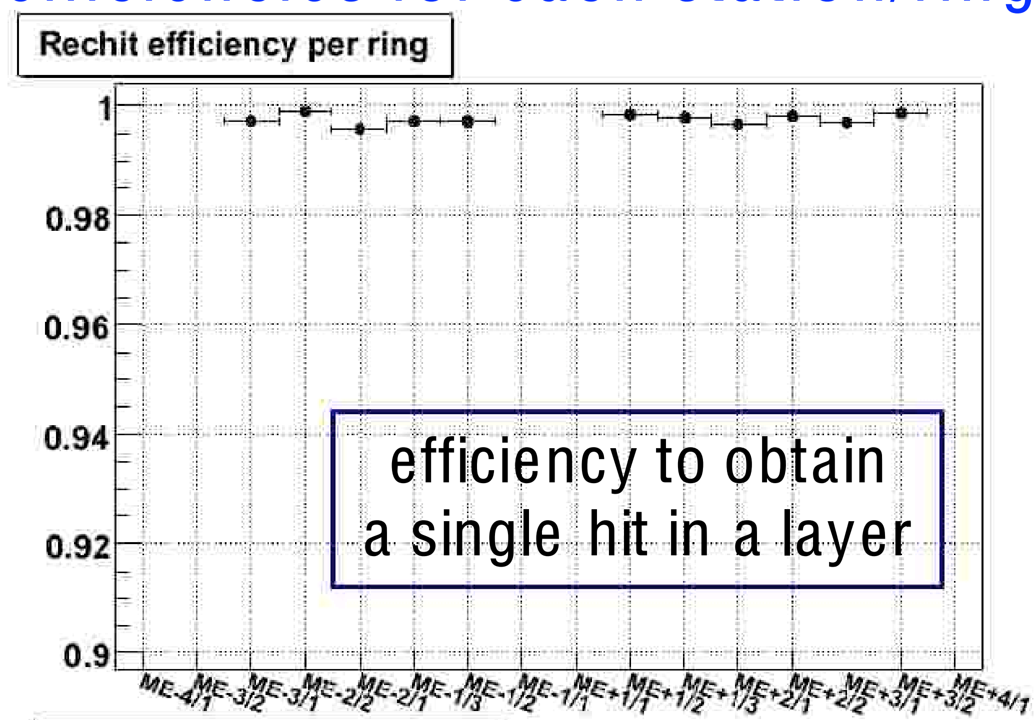

Endcap Muon CSC chambers performed well during cosmics run.

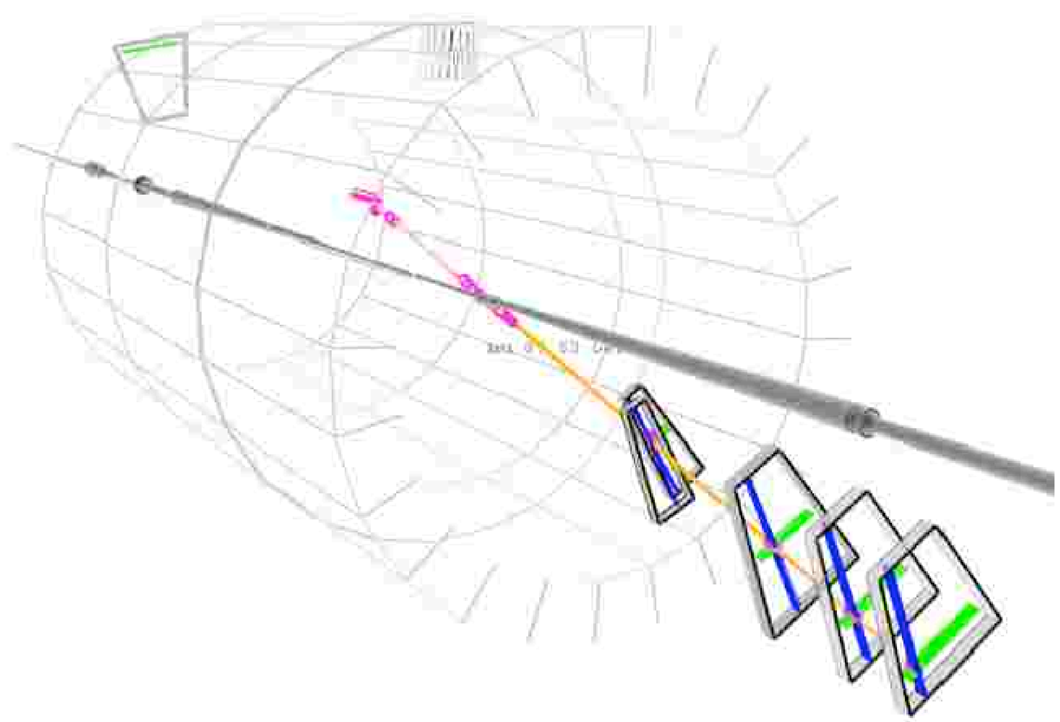

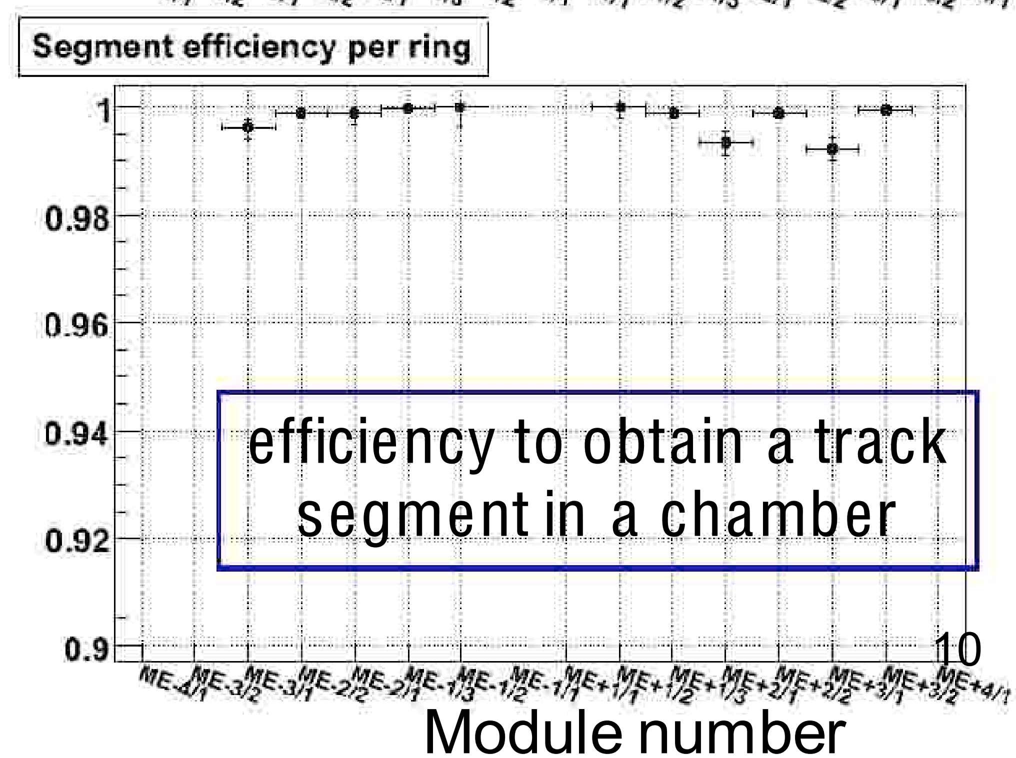

F. Cavallari, Elba 2009

from L. Ropelewski

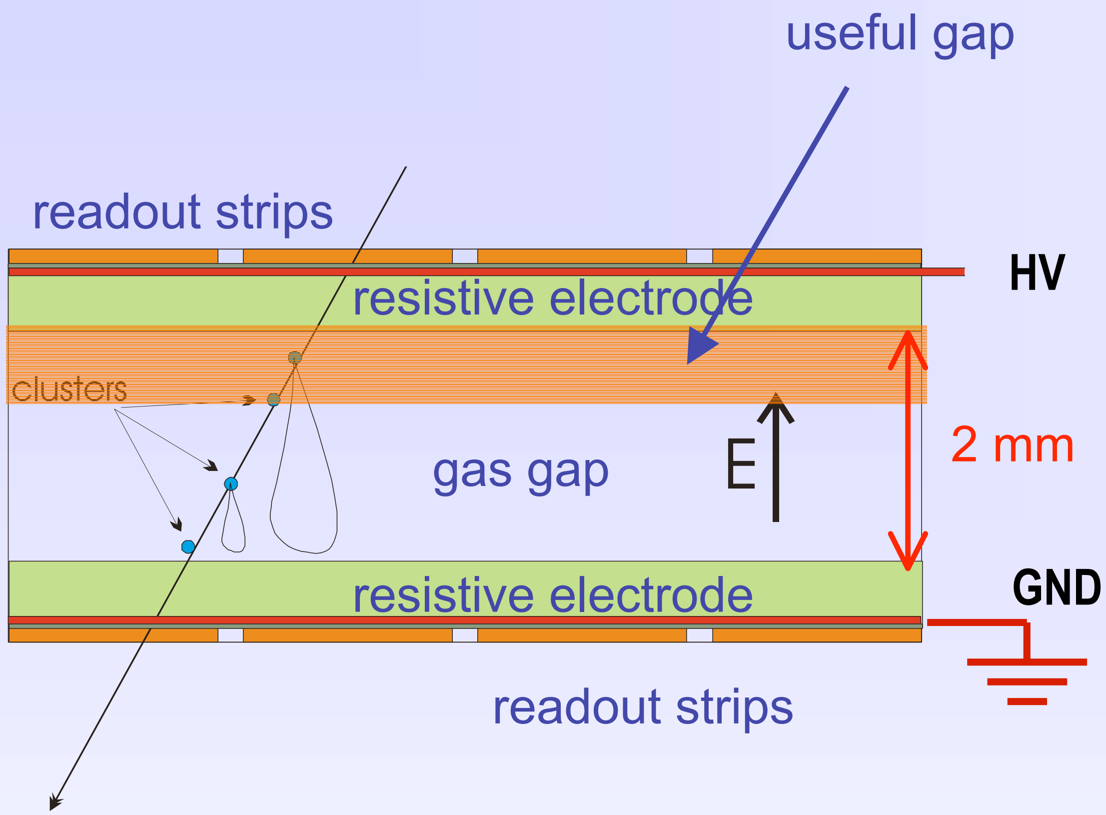

Rate capability strong function of the resistivity of electrodes in streamer mode.

MRPC

Multigap RPC - exceptional time resolution suited for the trigger applications

A. Akindinov et al., NIM A456(2000)16

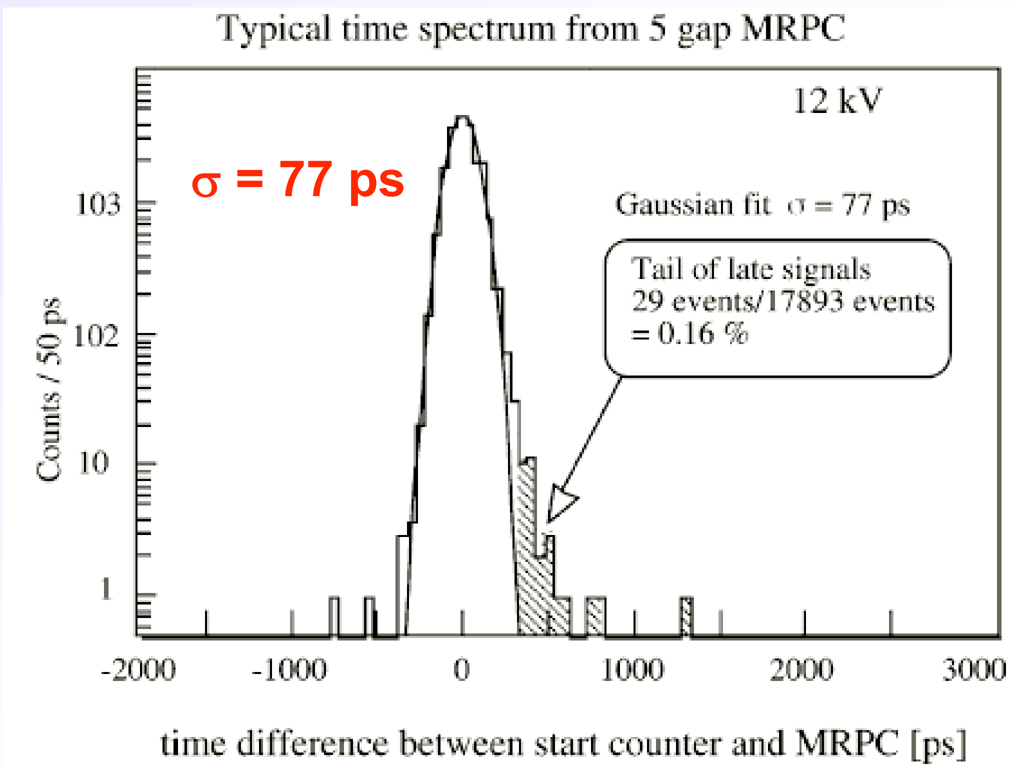

Time resolution

5. CMS Muon Barrel RPC Efficiency

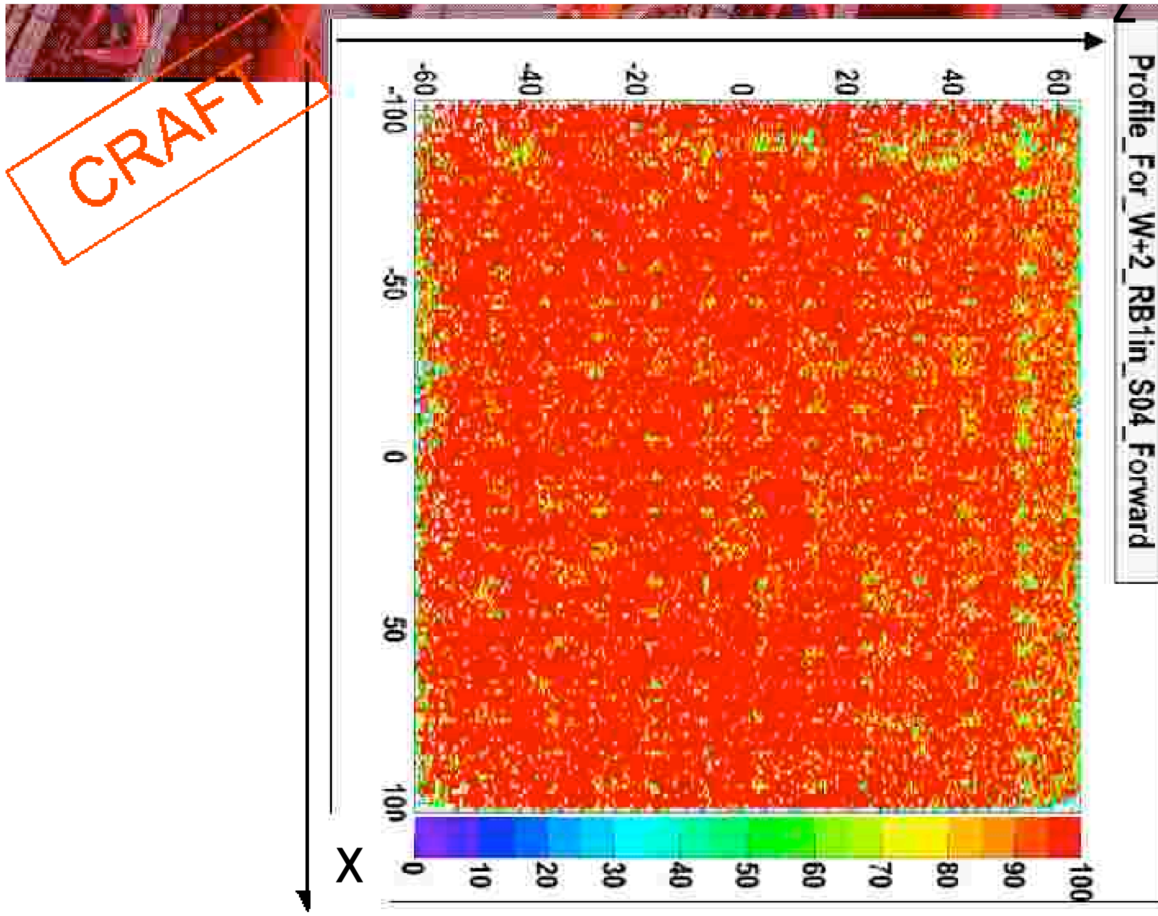

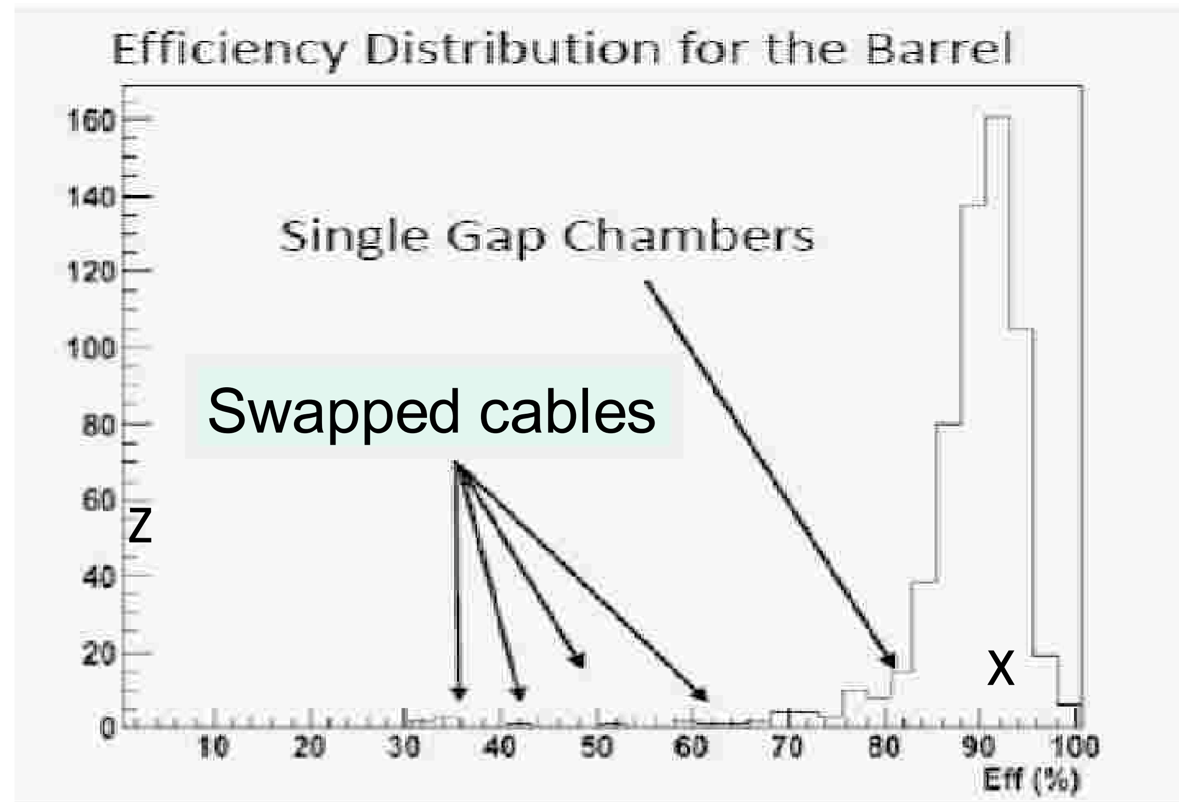

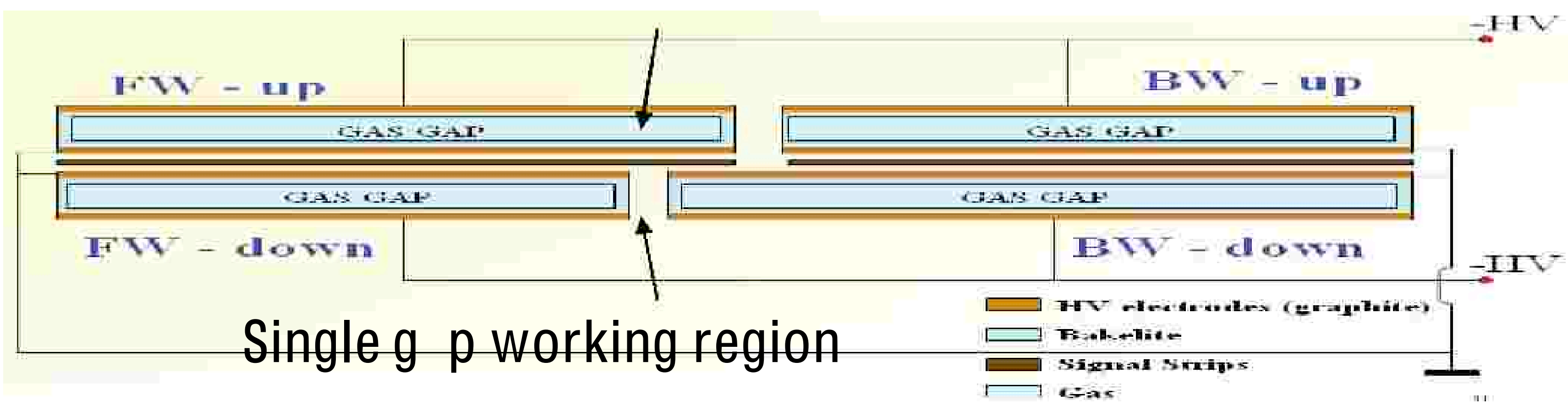

RPC efficiency vs impact point measured extrapolating DT segment on the RPC .
The low efficiency points (in step of 10 x 10 cm^2) are due to the spacers.
A slight degradation in efficiency is observed in the single gap zone.

POSTER

F. Cavallari, Elba 2009

The ATLAS Muon Spectrometer

Monitored drift tubes	**MDT**
- Coverage	$\lvert\eta\rvert < 2.7$ (innermost layer: $\lvert\eta\rvert < 2.0$)
- Number of chambers	1088 (1150)
- Number of channels	339 000 (354 000)
- Function	Precision tracking
Cathode strip chambers	**CSC**
- Coverage	$2.0 < \lvert\eta\rvert < 2.7$
- Number of chambers	32
- Number of channels	31 000
- Function	Precision tracking
Resistive plate chambers	**RPC**
- Coverage	$\lvert\eta\rvert < 1.05$
- Number of chambers	544
- Number of channels	359 000
- Function	Triggering, second coordinate
Thin gap chambers	**TGC**
- Coverage	$1.05 < \lvert\eta\rvert < 2.7$ (2.4 for triggering)
- Number of chambers	3588
- Number of channels	318 000
- Function	Triggering, second coordinate

A complex system:

- 4 different technologies (MDT,CSC,RPC,TGC)
- Large area (10,000 m^2)
- Many channels (1M)

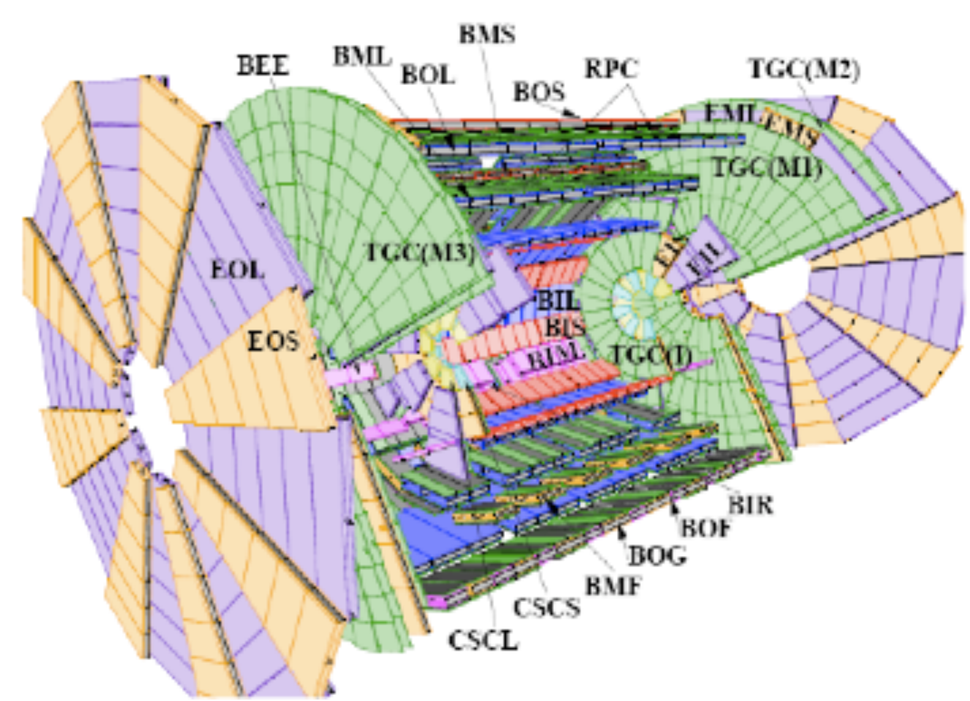

The ATLAS Muon Spectrometer

Difficult environment: Large magnetic field variations in toroid.

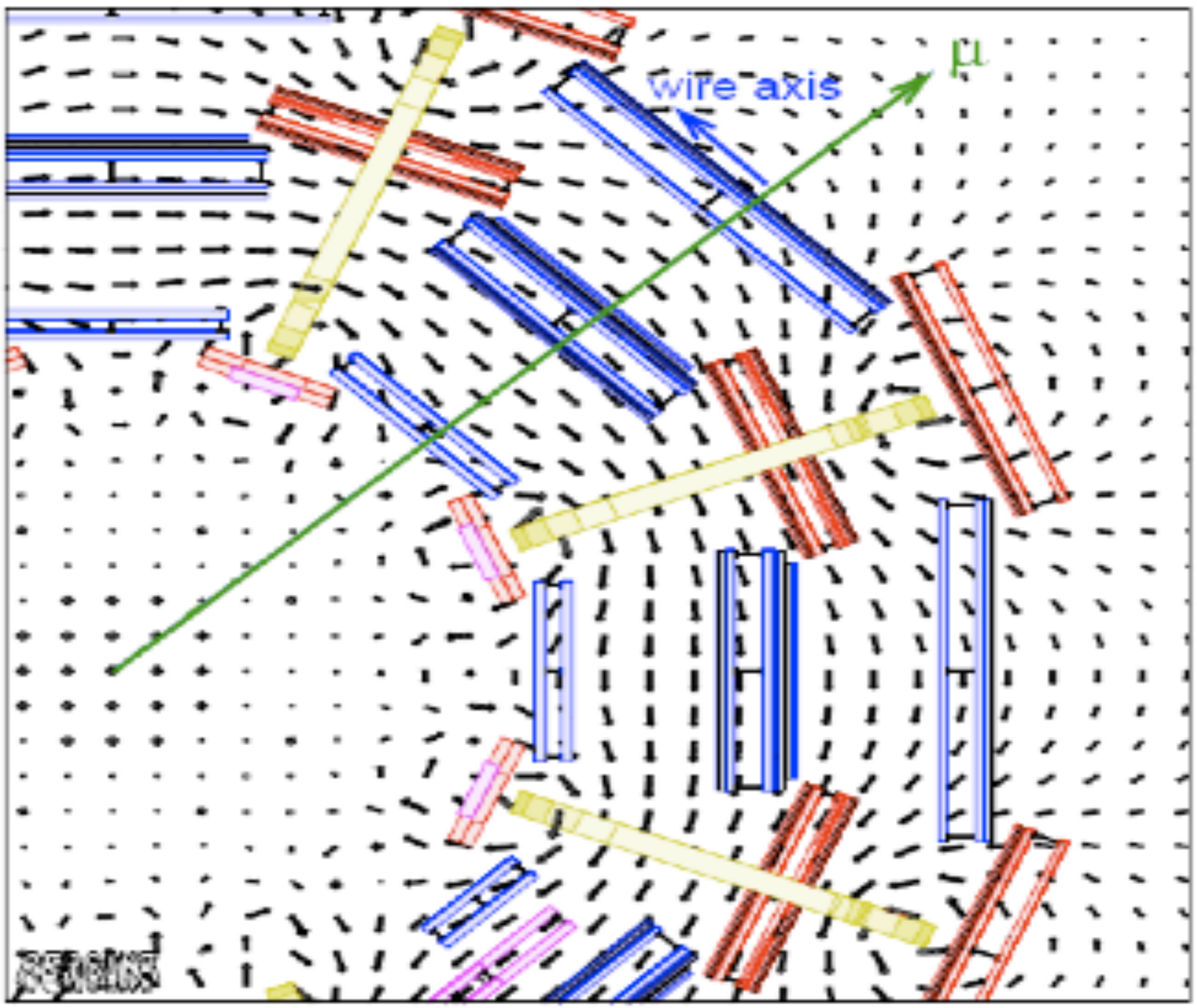

ATLAS Commissioning with Cosmics

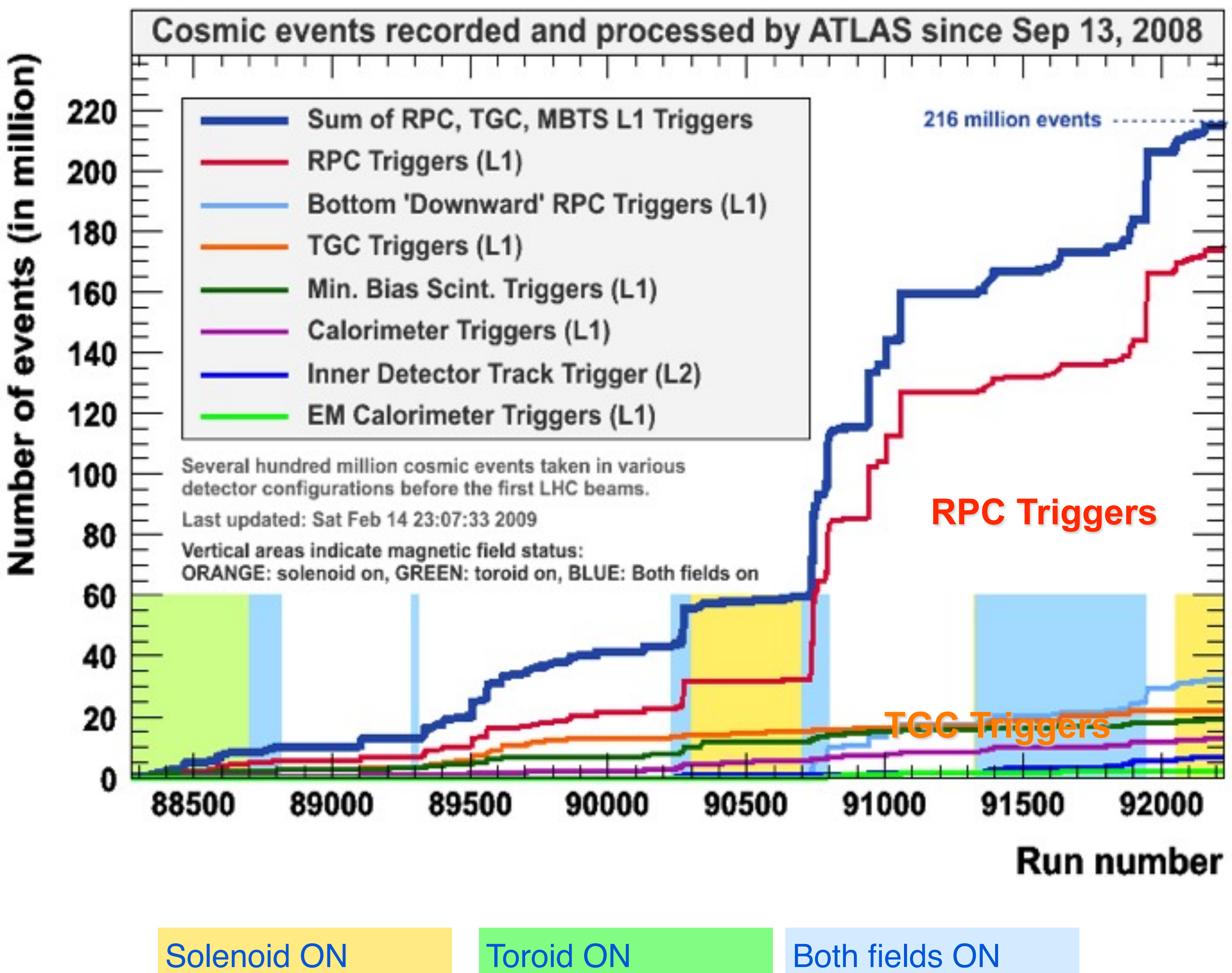

- High statistics collected in autumn 2008 (full ATLAS)
- Few high statistics runs studied in great detail
- Subdetectors runs in 2009: RPC runs in January
- "muon slice" runs at the end of April

5. ATLAS Resistive Plate Chamber Efficiency

Dead strips < 2%
Noisy channels < 1%

In 2008 problems with
- •Synchronzation
- •Gas
- •Temperature (reduced HV in top sectors)

Affected the overall efficiency (70% of trigger coverage)

Most of the problems were fixed during the winter shutdown, current trigger coverage is 95.5%

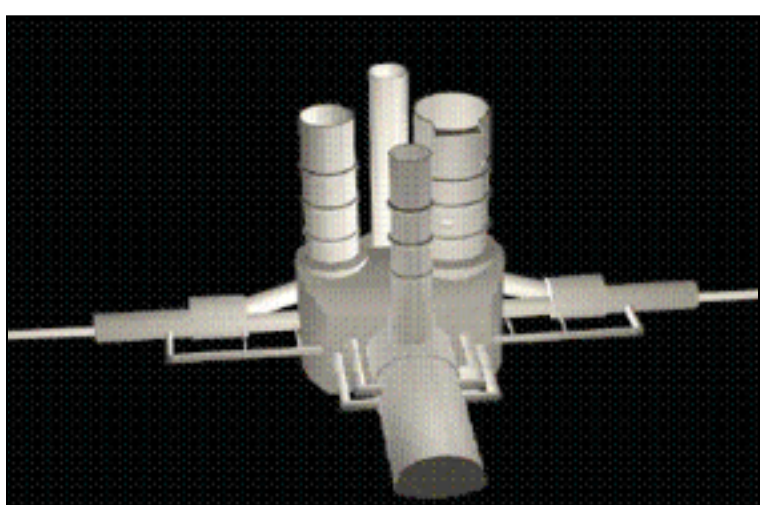

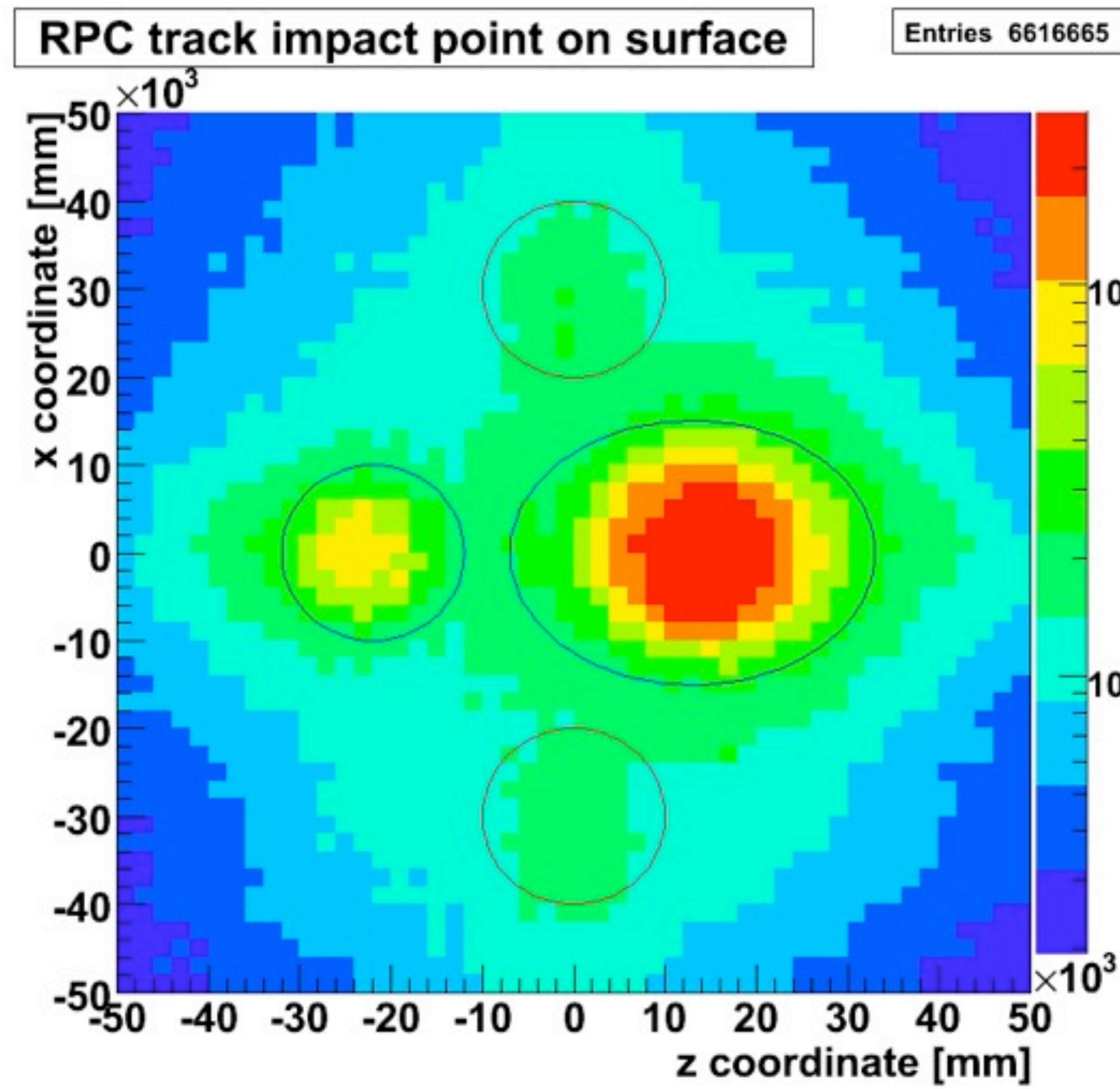

Access shaft of ATLAS cavern reconstructed in measurement.

5. ATLAS RPC Trigger Coverage

Low-pt trigger coverage

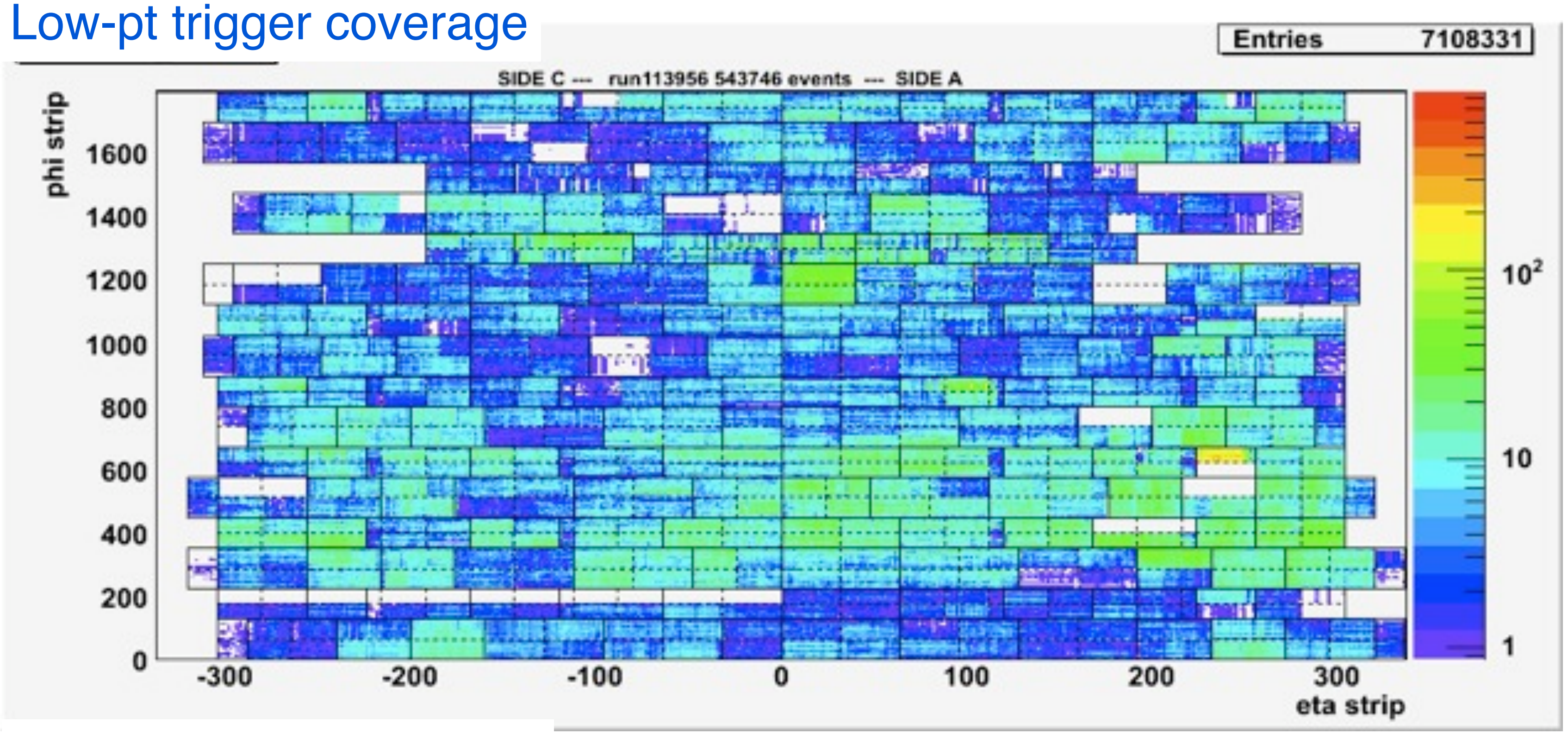

High-pt trigger coverage

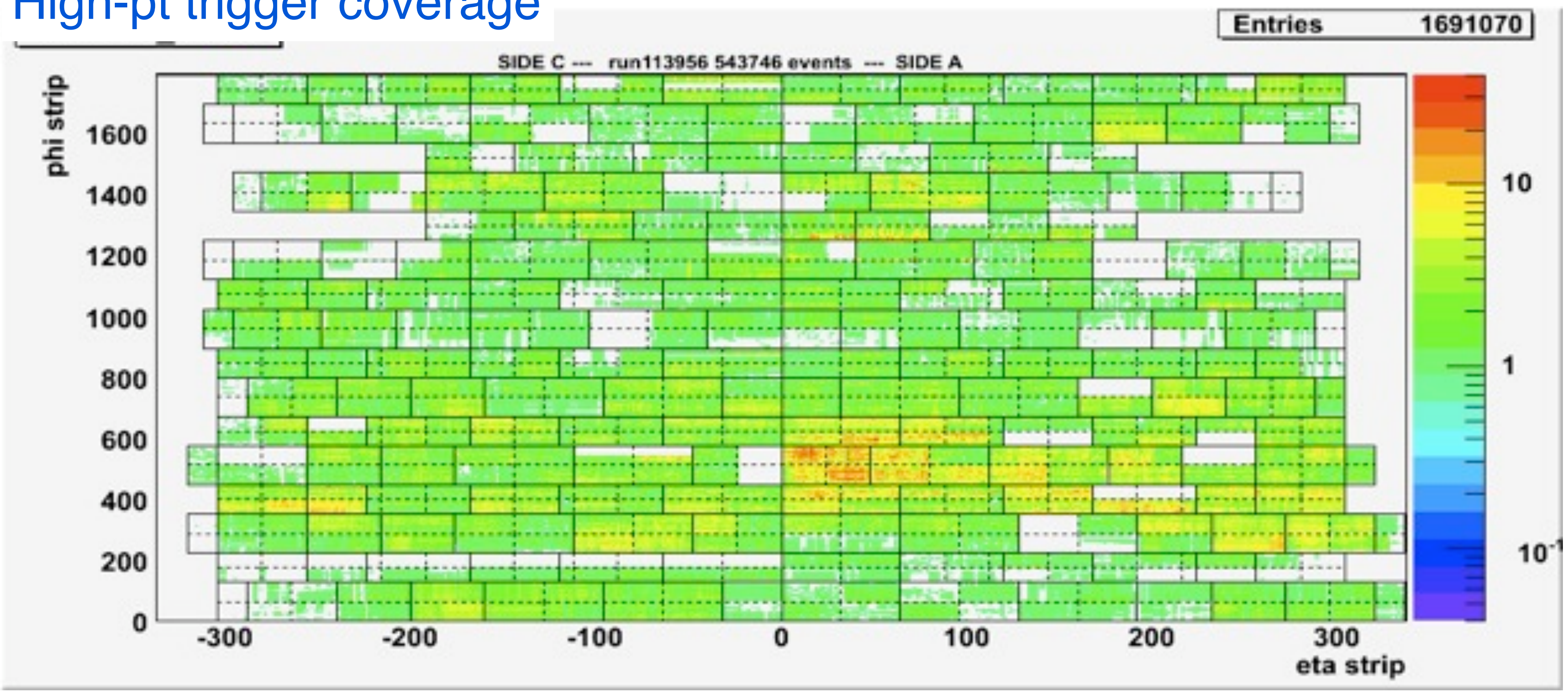

Hit maps of the strips involved in Low and High Pt triggers

- Commisioning ongoing
- Trigger coverage increased from 70% in 2008 to current 95.5% (better timing)
- Full detector for 2009 run.